Nature-Inspired and Sustainable Synthesis of Sulfur-Bearing Fe-Rich Nanoparticles

David O'Connor, Deyi Hou,* Qingsong Liu, Martin R. Palmer, and Rajender S. Varma*

ABSTRACT: Sulfur-bearing Fe-rich nanoparticles (SINPs) have been subject to increased levels of interest because of their catalytic properties and other features. However, with increasing interest in greener and sustainable practice, traditional engineered routes to SINP synthesis have become a concern owing to their high energy and resource demand as well as the use of potentially hazardous or environmentally harmful reagents. Here, we aim to bring attention to emerging and burgeoning research across a wide range of disciplines on the formation of both naturally occurring and synthetic SINPs. First, various SINP types are described, and their most important characteristics are outlined. Second, the natural mechanisms of SINP formation are evaluated and their environmental significance explained, predominantly in hydrothermal vents and lithogenic environments, in order to help inspire new approaches to engineered synthesis. Third, an appraisal of various synthetic approaches for SINP assembly is presented, with a focus on green synthesis methods. One exemplar is the use of nature inspired biosynthesis, which has been increasingly explored for the fabrication of cost-effective and environmentally friendlier SINPs. Finally, potential future research directions leading to more sustainable SINP synthesis are put forward.

KEYWORDS: Nanostructures, Nanomaterial fabrication, Green synthesis, Biosynthesis, Iron sulphides

INTRODUCTION

The International Organization for Standardization (ISO) define nanoparticles (NPs) as particles with dimensions that do not exceed 100 nm.[1] These particles possess physical and

chemical properties that differ from bulk materials; for example, they may display exceedingly high surface area-to-volume ratios, quantum effects, and semiconductor band gaps relating to their dimensions.[2] Thus, the application of NPs benefits many technologies and consumer products, including renewable energy technologies, personal care products, biomedicines, agrochemicals and water/soil environmental treatment processes.[3−5]

An expanding body of research pertaining to sulfur-bearing iron-rich nanoparticles (SINPs) has been of prime interest due to their utility in catalytic, electromagnetic, and optical applications and because of the natural abundance of SINP precursor material resources.[6−9] However, sustainability concerns persist regarding SINP manufacturing, including the associated environmental impacts and the desire to reduce production costs.[10] This has led to growing interest in the adoption of sustainable materials and green technological approaches.[11]

On the basis of research that extends across a wide range of disciplines and includes both naturally occurring and synthetic nanomaterials, researchers are increasingly generating innovative solutions to improve synthesis sustainability.[12] For example, the emerging "nature-inspired" design philosophy is based on copying natural formation mechanisms.[13] Such approaches have been particularly important in the development of improved synthesis methods associated with low secondary impacts.[14,15]

Herein, we examine both natural and engineered synthesis of SINPs in an attempt to provide an improved understanding of the formation of this class of NP and encourage the development of more sustainable SINP synthesis techniques. The structure of this perspective reflects the objectives of the review undertaken, which are as follows: (1) to review the various SINP types and outline their most important characteristics, (2) to evaluate the natural formation of SINPs, with the natural mechanisms of SINP formation and their environmental significance explained in order to encourage researchers to develop new nature inspired synthesis processes, and (3) to provide an appraisal of green synthesis methods. Finally,

suggested future research directions for the advancement of more sustainable SINP synthesis techniques are provided.

TYPES AND CHARACTERISTICS OF SULFUR-BEARING FE-RICH NANOPARTICLES

Different types of SINPs, which comprise various iron sulphide compounds, have received attention in recent years because of their characteristics, including their optical absorption coefficients and photovoltaic (PV) conversion efficiencies.[16–18] In this section, various SINP types and their characteristics are outlined, which are briefly summarized in Table 1 for reference.

FeS, Mackinawite and Troilite (Approximate FeS). Iron(II)sulfide (FeS) is not normally stable in its amorphous form. Cubic FeS_c has a cubic F43*m* structure and is not found in nature[19] because it readily converts to mackinawite.[20] Mackinawite, expressed in the formula FeS_m, comprises Fe atoms surrounded by four sulfur atoms in a nearly perfect tetrahedron structure,[21] forming a tetragonal P4/*nmm* structure.[19] It is a widespread metastable mineral in low-temperature aqueous environments, being the major FeS constituent precipitated from aqueous solutions.[31] In terms of its technological applications, mackinawite has seen much interest in environmental technology as a reducing reagent (e.g., for the dechlorination of chlorinated organic pollutants) and sorbent for divalent metals.[32]

FeS can also be found in nature as troilite (FeS_t), with a hexagonal *P62c* structure.[19] It is the stoichiometric end member of the pyrrhotite mineral group, having antiferromagnetic properties at ambient temperature.[22] Troilite forms in nature under strongly reducing environments and is less abundant in terrestrial environments than other pyrrhotite minerals, being only found at low concentrations where there are strongly reducing environments.[23] However, troilite is abundant in meteorites, and it may occur in massive forms (up to 5 cm crystals) in iron meteorites.[23] A characteristic of troilite is that when it is heated to above the

β-transition temperature (315°C), it is transformed from an antiferromagnetic structure to a paramagnetic structure with magnetic moment disordering (Figure 1), which is accompanied by a phase transformation to the NiAs subcell (1C).[23]

Pyrrhotite ($Fe_{1-x}S$). Pyrrhotite ($Fe_{1-x}S$, where x = 0 to 0.13) minerals are nonstoichiometric variants of FeS, which exist as monoclinic (e.g., *A2*/*a*) or hexagonal (e.g., *P6/mmc*) structures[19] or trigonal phases.[23] Pyrrhotite minerals are relatively abundant on Earth, being found in many geological settings.[19]

It is the ordered omission of Fe that produces superstructures that range from hexagonal to monoclinic.[24] The monoclinic structure (often denoted as Fe_7S_8, but with a wide compositional range) contains alternating layers of full iron sites and layers of sites with iron vacancies. Pyrrhotite with a hexagonal structure (i.e., the nickel arsenide (NiAs) structure) will distort into a monoclinic structure if the vacancy content is greater than 0.11 per formula unit.[25] The hexagonal form of Fe_7S_8 is stable and antiferromagnetic, whereas monoclinic pyrrhotite is strongly ferrimagnetic. Hexagonal pyrrhotite is known to naturally form in many geological settings, including deep-sea sediments associated with methane hydrates.[33] Hexagonal primary pyrrhotite can be partially oxidized when exposed to oxygen, forming iron-deficient secondary pyrrhotite.[23] Monoclinic pyrrhotite exists widely in reduced igneous rock and metamorphic rocks and can be transported to marine sediments as an erosional product. Once it is present in marine sediments, monoclinic pyrrhotite is an excellent provenance tracer. Notably, it is particularly common in extraterrestrial rocks.[34]

Because numerous pyrrhotite superstructures occur with varying iron vacancy arrangements,[35] they display various magnetic and electrical properties.[36−38] For instance, pyrrhotite minerals display a range of thermomagnetic behaviors depending on the precise composition.[25] The pyrrhotite Curie temperature is reported as 310−325 °C, depending on the composition, and is considered stable and ferrimagnetic at lower temperatures.[25] Impurities as

an isomorph substitute (e.g., incorporation of Ni) can significantly lower the Curie temperature value. When pyrrhotite is heated to greater than 325°C, the magnetic moment decreases dramatically, due to long-range magnetic moment disordering or vacancy disordering confined to different sites in alternating rows in each vacancy layer.[29] The structures of other $Fe_{1-x}S$ variants have partially filled Kagome net layers and Fe-filled layers stacked with long-range orders established along the c axis.[39] Several other pyrrhotite minerals, such as Fe_9S_{10}, $Fe_{10}S_{11}$, and $Fe_{11}S_{12}$, are generally hexagonal, antiferromagnetic, and only stable at temperatures below 209°C.[40]

Greigite (Fe_3S_4). Greigite (Fe_3S_4) has a cubic *Fd3m* structure[19] and is the iron sulfide counterpart of spinel magnetite (Fe_3O_4,); although electronic structure calculations show that greigite is a normal metal, magnetite is only half-metallic.[26] Greigite was first observed in clay layers, as grains and crystals, in drill cores retrieved in San Bernardino, California, USA,[27] but it is now known to be widespread in the natural environment, being mostly associated with fresh water systems, where it can be stable for millions of years.[41] Aquatic magnetotactic bacteria (MTB) have also been found to contain greigite, which they utilize to migrate along geomagnetic field lines.[42]

The unit cell of the stoichiometric inverse spinel greigite structure contains 32 sulfur atoms and 24 iron atoms,[27,28] with two sublattices of iron atoms with Fe^{3+} ions occupying tetrahedral A-sites and Fe^{2+} and Fe^{3+} ions occupying octahedral B-sites.[29] While greigite is thermally stable at ambient temperature, it will break down to form pyrrhotite when heated and slowly dissolves in hydrofluoric acid or warm hydrochloric acid.[27] The relative instability of greigite has resulted in it being less well studied than magnetite, but engineered greigite is now receiving greater interest owing to its complex magnetic properties.[30]

Band structure calculations have revealed a complex Fermi surface and the influence of relativistic effects. For example, two sheets of the Fermi surface disappear or reappear

depending on the direction of applied magnetization. This phenomenon enables spintronic engineering at a single compound level, an advancement over traditional heterostructures.[26] However, the magnetic properties of engineered greigite are sensitive to synthesis conditions, and knowledge of these properties is incomplete.[43] It is also difficult to synthesize pure greigite because most methods will also produce other iron sulphide impurities, such as mackinawite and pyrite.[44] This is usually discovered by observing X-ray diffraction patterns, which often reveal nongreigite peaks. Nevertheless, pure synthetic greigite has been extensively investigated by a series studies by Chang and his colleagues.[45−48]

For bulk greigite, the expected saturation magnetization (M_s) at room temperature is 4 μ_B per formula unit (f.u.); however, M_s values are usually measured to be less than 2.5 μ_B/f.u., implying poor purity (i.e., mackinawite and pyrite impurities, see above).[49] The parameter of exchange interaction (JAB) between Fe ions in (A) and (B) sublattices is estimated at 1.03 meV, and no low-temperature magnetic transition is present.[29]

Greigite SINPs have the potential to be used as an anode material in lithium-ion batteries (LIBs)[50] and as intermediates in solar cells.[44] Interest in the use of greigite in LIBs has been increasing because of its high theoretical capacity of 785 mAh/g, which is more than twice that of conventional graphite (372 mAh/g).[49] It is also noteworthy that greigite is nontoxic and abundant on Earth. Furthermore, greigite SINPs hold potential applications in the areas of hydrogen storage, magnetic guided delivery of drugs, and for cancer hyperthermia applications.[51,52]

Greigite NPs have also been used as an enzyme mimetic to catalyze chemical reactions because natural enzymes are vulnerable to changing acidity, temperature, and inhibitors.[53] The intrinsic enzyme mimetic activity is similar to natural peroxidases and has been exploited to develop novel immunoassay methods. Greigite has a stronger affinity than Fe_3O_4 in peroxidase-

like behavior, which suggests that greigite SINPs have good potential for medical detection applications.[53]

Pyrite (FeS_2). Pyrite has the composition FeS_{2p}, forms in a cubic *Pa3* structure, and is one of the most abundant minerals of the Earth's surface[19] (FeS_2 with an orthorhombic crystalline structure is known as marcasite). Pyrite has many uses for modern technological processes. For example, its high adsorption coefficient ($\alpha > 10^5$ cm^{-1} for hv >1.3 eV) and band gap (0.8−0.95 eV) make it useful as an PV absorber material.[22,54,55] Pyrite-containing devices have high quantum efficiency (>90%), high photocurrents (>40 mA cm^{-2}), and low photovoltages (<200 mV).[56–58] Pyrite nanocrystals can also be deposited on flexible substrates such as solar ink or paint in order to provide large surface area PVs.[59] Importantly, cobalt can also be substituted in cubic pyrite nanocrystals ($Co_xFe_{1-x}S_2$) as nanoscale thin films to enable switching from p-type to n-type semiconductors between x = 0.16 and 0.21.[60] Compared to traditional single crystal pyrite, pyrite NPs offer cost-effective and highly scalable options for such applications. As a PV material, pyrite NPs have the benefit of wide natural abundance and relatively low toxicity to humans. Moreover, if some of the vast amounts of pyrite discarded as a mining waste could be captured for use in solar PV and photoelectrochemical cells,[54] it would not only be a waste-to-resource gain but would also help reduce the impacts of acid mine drainage caused by pyrite oxidation.

Other promising uses for pyrite SINPs are in high-performance cathodes for energy storage, e.g., lithium-ion batteries (LIBs), due to their long shelf life and relatively high capacity,[55] and in wastewater treatment due to its high catalytic activity toward organic pollutants. For example, pyrite SINPs show high photocatalytic activity toward organic dyes (e.g., methylene blue and Synazol Yellow K-HL), due to the creation of reactive oxygen species via a photo Fenton-like process.[61]

Multimetallic SINPs. Multimetallic SINPs have been explored to address issues arising among the various SINP types. For example, while pyrite has great potential as a PV material, due to its high adsorption coefficient and band gap, it also suffers from crystal defects arising from sulfur vacancies,[62,63] which may be mitigated by the use of bimetallic pyrite.

Naturally occurring bimetallic FeS minerals are also found in sedimentary, hydrothermal, and igneous environments. For instance, arsenic can be incorporated into iron sulfide as arsenian pyrite (referred to as arseno-pyrite) in the form of As^{3+}-pyrite (As substitutes for Fe) or As^{1-}-pyrite (As substitutes for S).[64] Arsenian pyrite is an important host of gold in hydrothermal ore deposits, as well as a source of arsenic pollution in the natural environment.[65,66] While As^{3+}-pyrite tends to form under oxidizing conditions, As^{1-}-pyrite will form under relatively reducing conditions. As^{3+}-pyrite formation on pure pyrite depends on the crystal size, with larger crystal sizes containing higher arsenic concentrations.[64]

Other bimetallic iron sulfide minerals found in nature include pentlandite ($[Fe,Ni]_9S_8$), which is a common mineral in chondritic meteorites, polar micrometeorites, and chondritic interplanetary dust particles (IDPs).[67] Bimetallic $CuFeS_2$, which is found in volcanogenic massive sulfide deposits among other environments,[68] may offer greatly increased efficiency in the conversion of waste heat into energy. For example, synthetic ∼6.4 nm bimetallic $CuFeS_2$ can display thermoelectric values ∼77 times higher than bulk chalcopyrite.[69]

Core−Shell SINPs. Various core−shell SINPs have been developed and synthesized for various technological applications. For example, core−shell Au/FeS NPs with polyethylene glycol coatings have been developed in which the Au component functions as a radiosensitizer in medical applications.[70] The FeS component of these SINPs provides contrast to enhance magnetic resonance imaging and photoacoustic imaging, and the coating enables higher dosages without the associated metal toxicity to patients.

In environmental applications, methods have been developed for large-scale synthesis of core−shell FeS NPs, involving FeS shells on zerovalent iron (ZVI) NPs.[71,72]

FORMATION OF SINPS IN NATURAL ENVIRONMENTS

Natural sulfur-bearing Fe species occur in many natural environments, with iron sulfides being among the most extensively dispersed reduced S species found on Earth. For example, sulfur-bearing Fe-rich minerals are a common constituent of the lithosphere, being found in many types of geological bodies, such as ancient sedimentary rocks, modern sediments, mineral deposits, and submarine hydrothermal vent deposits. As well as the lithosphere, naturally formed NPs have also been discovered in the troposphere (and even higher), the hydrosphere (oceans, lakes, rivers, and groundwater), and the biosphere (principally microbes, but also in higher organisms including humans),[73] and even on asteroids.[74] In this section, we explore these naturally forming S-bearing Fe-rich NPs in order to provide inspiration for the development of new engineered synthesis techniques.

Lithosphere. Sulfur−iron reactions play key roles in the geochemistry of the lithosphere, from low-temperature (<100°C) sedimentary systems[75,76] and intermediate-temperature (100−400°C) hydrothermal sulfide deposits that form large ore bodies[77] to high temperature (up to 1000°C) igneous and metamorphic rocks.[78] While SINP formation has not been reported as primary phases in high-temperature rocks, SINPs may form in low- to intermediate-temperature systems by a variety of processes, including dissolution-precipitation reactions or via mechanical breakdown of bulk iron sulfides and other weathering processes.[11,73] The volumetrically most important Fe−S minerals in these settings are pyrite, mackinawite, and greigite.

In natural lithogenic reactions (Figure 2), Fe^{2+} is released into solution by the dissolution of Fe-bearing minerals (i.e., ferric (hydr)oxides) under reducing conditions, which

occurs largely by microbe-facilitated dissimilatory Fe reduction or by abiotic reactions involving dissolved reductants.[79] In reducing conditions, sulfur will tend to exist as sulfide (i.e., HS^- at pH > 7). The reduction of sulfate to sulfide is also commonly biologically mediated, although it may also occur by interaction with reduced iron species. H_2S is a slightly soluble microbial product that acts as a weak acid, yielding HS^- (pKa = 6.9) and S^{2-} (pKa = 11.96).

A variety of SINPs can form via dissolution−precipitation reactions, including mackinawite (FeS) as a nanocrystalline or amorphous phase.[81−83] FeS species may react with dissolved polysulfides to form pyrite,[79] via microbial formation of mackinawite on iron oxide particles.[84] High-resolution transmission electron microscopy (TEM) observations of materials isolated from marine sediments have revealed mackinawite nanocrystalline structures containing 10−15 atomic layers.[85]

During diagenesis, greigite will grow if dissolved Fe and S_2 are available. Its formation and preservation rely on various factors including the availability of organic carbon, S_2 production, and presence of reactive Fe.[43] Greigite is a precursor in the Fe−S system to pyrite formation (Figure 2).[80,86,87] Natural incorporation of trace elements/impurities into natural SINP structures can occur in a range of low- to intermediate-temperature environments.[65,88−90] Of these, one of the most notable involves the incorporation of As. This occurs by substitution of As^{1-} for S in the sulfide unit of pyrite (thus forming arsenopyrite, $Fe(As,S)_2$), or under nonequilibrium kinetically controlled environmental conditions, As^{3+} can also be incorporated into pyrite by substituting for Fe^{2+}.[64]

Microbial Processes. In oxygen-absent environments, anaerobic bacteria use alternatives to oxygen as electron acceptors. Sulfate-reducing bacteria (SRB), which are ubiquitous in anaerobic water columns and subaqueous sedimentary environments, play a key role in iron−sulfur mineralization in sedimentary environments, including the formation of mackinawite, pyrite, and greigite. The initial step in the formation of bulk iron sulfide minerals

involves the formation of SINPs, with the cell wall being coated with nanosized iron sulfide precipitates (Figure 3).

Dissimilatory metal-reducing bacteria can respire elemental sulfur (S^0) as an alternative electron acceptor in alkaline pH environments, leading to mackinawite formation in alkaline groundwater systems. In this case, microbial and abiotic processes are coupled. For example, sulfur reduction by SRB leads to iron(III) reduction by an abiotic reaction with sulfide, which, in turn, leads to further sulfur reduction by SRB.[92] Thus, sulfur is recycled for multiple rounds of SRB reduction (Figure 4).

In experiments conducted at pH 7, nanoscale mackinawite rims have been observed on lepidocrocite crystals, with interfacial magnetite forming as a steady state layer as a product of lepidocrocite−mackinawite interaction. During the initial stages of these reactions, Fe^{2+} forms in excess to FeS. The fraction of excess Fe^{2+} increases at lower sulfide to surface site ratios, suggesting kinetic decoupling of sulfide oxidation and Fe^{2+} detachment from lepidocrocite. This may be due to sulfide donating electrons to lepidocrocite at a faster rate than stoichiometric amounts of FeS production. After 2 days of experimental observations, Fe^{2+} and S^0 levels decreased, resulting in pyrite formation dislocated from the lepidocrocite surface, as well as traces of magnetite. The absence of dissolved sulfide under these conditions suggests the formation of polysulfides, which are precursors for pyrite formation.[84]

In addition to SRB, iron-reducing bacteria (IRB) play an important role in SINP formation. For example, IRB in acid mine drainage facilitate iron sulfide formation under anoxic conditions.[93] Again, this observation may aid in devising a biosynthesis method for SINP production. Magnetotactic bacteria (MTB) facilitate the formation of nanoscale ferromagnetic greigite (Fe_3S_4), mackinawite (tetragonal FeS), and tentatively, cubic FeS.[20] The mackinawite converts to greigite within the MTB by rearrangement of the Fe atoms; hence, MTB are responsible for magnetic SINPs production in some sediments.[91,94] MTB also produce

magnetosomes containing single-domain magnetite particles or single-domain greigite particles.

It should be noted that there can be notable divergence in the characteristics between different types of bacterially formed SINPs. For instance, SRB produced SINPs that possess a strong adsorption potential for a wide range of metal ions involve the inclusion of materials not normally precipitated as sulfides, while SINPs produced within magnetosomes are relatively pure.[91] The great diversity of microbes in natural systems means that their role in formation of SINPs under a wide range of conditions is far from fully understood. For example, it has been observed that *Thiobacillus denitrificans* can oxidize pyrite SINPs to Fe^{3+} and SO_4^{2-} in the presence of NO_3^-,[95] whereas samples lacking *Thiobacillus denitrificans* showed no oxidation effects. A key factor in this oxidation process is the nanoscale size of the pyrite SINPs, with this fraction being preferentially oxidized, whereas larger pyrite crystals remained intact. This suggests a significantly higher bioavailability of nanoparticulate minerals compared to larger mineral phases.

Submarine Hydrothermal Vents. High-temperature submarine hydrothermal vents are key sources of oceanic Fe.[96] Although much of the Fe that initially emerges from the vent orifice is in the form of dissolved Fe^{2+}, as the greater than 300°C reduced fluids cool and mix with oxidized ambient seawater, the Fe rapidly oxidizes, and a proportion of the dissolved Fe precipitates as $Fe(OH)_3$. Because hydrothermal fluids also contain high concentrations of dissolved reduced S, polymetallic sulfides also precipitate (including nanosized particles) as the vent fluid cools. Indeed, as much as 10% of the total Fe emitted by vent fluids may consist of SINPs.[97] In addition, pyrite SINPs (<200 nm) can form within the high-temperature−high pressure environment of an up-flow zone of hydrothermal vents before discharging to the ocean.[97] Overall, hydrothermal vent-derived SINPs vary in shape and size, with typical aggregate diameters of 50−350 nm.[98] Hence, while coarser and denser particles settle to the

seabed within the immediate vicinity of the vent site, finer grained particles may be carried by buoyant hydrothermal plumes (Figure 5).[97,99,100] They may then be transported for 100s to 1000s of kilometers by bottom water currents.[99]

Laboratory experiments have suggested that the stable dispersion of hydrothermally generated SINPs is aided by the slower oxidation kinetics (by several orders of magnitude) of pyrite SINPs relative to coarser-grained materials.[100] In mimicking hydrothermal vent conditions, engineered SINPs have been manufactured in the laboratory by heating dissolved Fe and H_2S together at 140°C, followed by rapid quenching at 0°C.[98] It is notable that the experimental studies incorporating powdered SiO_2 in the reaction mixture yielded SINPs that were closest in mineralogy and morphology to those found at hydrothermal vents. It has been suggested that this is because the silica particle surfaces create a favorable environment for pyrite nucleation, and it is noteworthy that both dissolved and particulate SiO_2 are major components of submarine hydrothermal systems.[98]

Paleoenvironmental Role. On the tectonic time scale, global sulfur and carbon cycles are well coupled and thus provide important environments for biological activities. Formation of pyrite via bacterial sulfate reduction can result in very negative $\delta^{34}S$ values owing to preferential utilization of ^{32}S by SRB. Studies have revealed large changes in $\delta^{34}S$ values over the last 550 Ma. Such long-term variations could be due to pyrite burial in the sedimentary reservoir.[101,102] In contrast, short-term variations in $\delta^{34}S$ values could relate to vertical heterogeneity (e.g., ocean stratification).[103]

Naturally formed greigite plays a role of interest in paleomagnetic and environmental magnetic studies.[77,104−106] On an orbital time scale, the formation and preservation of greigite can be modulated by ocean ventilation and variations in redox conditions caused by sea level changes. For example, sedimentary cores extruded from the South China Sea have revealed that fine-grained greigite dominated during glacial periods under anoxic conditions owing to

disconnection between the South China Sea and the Indian Ocean.[107] In contrast, ventilation becomes rigorous during glacial periods, and coarser-grained detrital (titano) magnetites are prevalent.

Continental shelves bridge the continent and ocean. Sediments in these regions are sensitive to sea level variation, with redox conditions changing rapidly with respect to the fast sea level changes. This can cause thick layers of greigite to occur. For example, a thick (~8 m) laterally distributed layer of greigite occurred during the marine isotope stages 17−13 within the scope of the Yellow Sea Warm Current from the Chinese Yellow Sea.[108] The occurrence of greigite corresponds to enrichment by the trace element cadmium (Cd), which indicates that a weak sulfidic condition was accomplished with trace levels of freely dissolved H_2S. Studies have shown that Cd^{2+} has faster water exchange reaction kinetics than Fe^{2+}; therefore, CdS precipitates prior to FeS formation and subsequent pyrite formation.[109] CdS formation would consume a certain amount of S and cause weak sulfidic conditions. This seems to favor the formation of greigite rather than pyrite. Direct evidence has been put forward showing that Cd concentrations peak at the redox boundary rather than a full reductive environment.[110]

Environmental Fate. Pyrite is the most abundant iron sulfide mineral in the lithosphere, yet its transformation in natural environments is not fully understood. Iron sulfides may exist buried within anaerobic sediments and rocks for millions of years before they are transported to oxygenated submarine and subaerial environments, where they can be oxidized by nitrate, Fe(III) oxides, or MnO_2 as electron acceptors.[111] These processes are sometimes exploited by the mining industry to produce copper from low-grade ores,[112] but pyrite oxidation also generates potentially harmful sulfuric acid (e.g., acid mine drainage).[112] In anoxic geological reservoirs, pyrite can be stable almost indefinitely.[111] However, ferric iron can oxidize pyrite,[113,114] and anaerobic pyrite oxidation by nitrate as an electron acceptor has been observed in natural sediments.[115,116]

There is much uncertainty regarding the environmental fate of SINPs and the full role that these NPs play within the natural environment, with physicochemical, macromolecular, and biological pathways all contributing.[117] For example, hydroxyl radicals formed as products of FeS oxidation can lead to oxidation and increased mobility of toxic As.[118] SINPs also display higher reactivity in microbial processes compared to bulk materials. For example, pyrite SINPs are readily oxidized to ferric iron and sulfate by microbial processes, with a closed recovery of electrons in pyrite oxidation and nitrate reduction reactions.[95]

Space Weathering. The first sulfur−iron species formed in the early solar nebula is believed to be stoichiometric FeS (troilite).[119] However, chondritic IDPs, which represent the earliest formed material available for study, contain abundant iron sulfides with more pyrrhotite than troilite. This suggests pyrrhotite to be an important nebular condensate phase caused by "space weathering", which altered the troilite surface.[120] SINPs have also been found on extraterrestrial materials returned to Earth from the 25143 Itokawa asteroid.[74] In this case, surface alteration was discovered on half of the particles examined, with SINPs being present in 5−15 nm layers on surfaces of olivine, low-Ca pyroxene, and plagioclase. These likely stemmed from vapor deposition. Some SINPs embedded in the surface of the olivine substrates show lattice fringes not consistent with troilite and pyrrhotite, likely due to the presence of Mg accompanied by SINPs.[74]

ENGINEERED SINP SYNTHESIS

A wide range of different synthesis procedures and approaches have been developed in recent years for the fabrication of engineered SINPs (Table 2). The main approaches include "bottom-up" wet chemistry or "top-down" mechanical approaches, by which SINPs of different sizes, shapes, and compositions can be produced. An outline of various synthesis approaches is provided in this section, but the reader should refer to the original publications for details of

specific synthesis methods. It should be regarded that SINPs of certain stoichiometries are sometimes rather difficult to synthesize precisely due to the complexity of the Fe−S system phase diagram (Figure 6).

Solvothermal and Hydrothermal Methods. Solvothermal and hydrothermal methods are commonly used to fabricate various types of engineered NPs and can be applied to produce high-quality SINPs. The most common reducing agents for solvothermal methods include dithionite and borohydride. Dithionite is widely used in research and industry because it is a relatively low-cost substance that decomposes in aqueous solution to form hydrogen sulfide (H_2S), which in the presence of dissolved Fe^{2+} leads to the precipitation of iron sulphide SINPs.[143,144] However, unintended precipitation products of solvothermal methods may cause impurities that need mitigation. A slight excess of sulfide can help prevent soluble Fe^{2+} from precipitating as iron hydroxide in mackinawite SINP synthesis.[32]

Pyrite SINPs. Pyrite SINPs of various morphologies can be formed by solvothermal and hydrothermal methods. For example, single-phase pyrite SINPs of crystallographic purity and good size uniformity (2−5 nm) can be formed using $FeCl_2 \cdot 4H_2O$ (1.3 mmol) in dimethyl sulfoxide containing thioglycolic acid, with $Na_2S_2O_3 \cdot 5H_2O$ added under continued stirring and N_2 purging. FeS_2 NPs form if the temperature is raised to the boiling point, which can then be further crystallized under reflux.[55] This method can be modified to produce pyrite SINPs of different morphologies. Nanowires and nanosheets can also be synthesized using the same precursors with only a slight modification of the method.[145]

The synthesis of FeS_2 SINPs with nanorod-type morphologies can be achieved using a solvothermal process involving FeS_2 in ethylenediamine to produce SINPs of 20−50 nm in diameter and up to 1000 nm in length.[146] The precise morphology depends on the type of solvent used (Figure 7). Colloidal pyrite SINPs can be produced by injecting a sulfur-diphenyl ether solution into an $FeCl_2$-octadecylamine solution at 220°C.[54] Pyrite SINPs have also been

synthesized using iron(II) chloride tetrahydrate ($FeCl_2 \cdot 4H_2O$) and sodium thiosulfate pentahydrate ($Na_2S_2O_3 \cdot 5H_2O$) as precursors.[61]

In single-stage hydrothermal synthesis using a mixture of $FeSO_4$ with $Na_2S_2O_3$ and elemental S in water at 90−280°C, lengthy reaction times (24 h) favor the formation of pyrite crystals.[147] The resulting SINPs have an average particle size of ∼500 nm and are AB_2 cubic structured (space group *Pa3*, lattice constant a = 5.4151 Å, and Wyckoff parameter *u* = 0.3868). SEM images (Figure 8) illustrate a well-crystallized polycrystalline pyrite form.

The possible mechanism for the formation of pyrite SINPs from $Na_2S_2O_3$, elemental S, and $FeSO_4$ was reported as follows:[147]

$$Na_2S_2O_3 + H_2O = H_2S \uparrow + Na_2SO_4$$

As H2S is saturated in aqueous solution, the following equilibria exist:

$$H_2S \leftrightarrow H^+ + HS^-$$

$$HS^- \leftrightarrow H^+S^{2-}$$

The added elemental S is deoxidized by hydrosulfuric acid, which releases H_2S:

$$S + 2H^+ + 2e \leftrightarrow H_2S\uparrow$$

FeS is formed as the added $FeSO_4$ releases Fe^{2+} ions, and the ionic products of Fe^{2+} and S^{2-} exceed the solubility product of FeS. The solubility of H_2S is low, so it exists mostly as a gaseous phase, driving the following pyrite forming reaction:

$$H_2S + FeS = FeS_2 + H_2$$

There are various factors that influence the size and morphology of pyrite SINPs produced by hydrothermal methods using different S sources.[98] Synthesis procedures using elemental S proceed via polysulfide and produce mainly octahedral pyrite particles, whereas synthesis using H_2S proceed via FeS and H_2S and produce much smaller NPs with diverse morphologies, including cubes and framboids. The synthesis of high-quality, phase-pure, and single-crystalline pyrite nanoparticles via the hydrothermal route has been accomplished

wherein the reaction time and S:Fe molar ratio play important roles in the quality and morphology of FeS_2 nanocrystals produced. A high sulfur to iron molar ratio and longer reaction times are beneficial for this purpose.[148]

FeS SINPs. Synthesis of (approximate) iron sulfide (FeS) NPs can easily be achieved by wet chemical reduction and the formed FeS SINPs separated by filtration. A tentative chemical reaction for such a process is as follows:[149]

$$2Fe(NO_3)_3.9H_2O + 3C_4H_4Na_2O_6.2H_2O + 2Na_2S_2O_3.5H_2O \rightarrow$$

$$FeS + 6NaNO_3 + 2Na_2SO_3 + C_4H_4Na_2O_6\ (aq)$$

The synthesis of FeS SINPs with needle-like morphology can be achieved via the Schlenk technique under a N_2 atmosphere[130] and autoclaving the solution at 150°C for 12 h followed by centrifugation. Colloidal nanosheets of mackinawite (FeS) can also be synthesized by coprecipitating an amorphous Fe-S precursor, which is first formed by rapid injection of Na_2S into a $FeCl_2$ solution, followed by centrifugation, sonication of the precipitate in ethylene glycol, and heating in an autoclave to 200°C. The resulting product has lattice constants of a = 3.674(3) Å and c = 5.0354(3) Å, with the nanosheets irregularly faceted of length 100 nm to greater than 1 mm and ∼30 nm thicknesses with the surface normal oriented along the [0 0 1] direction.[24] Variations of the synthesis procedure can also produce Fe/FeS SINPs of 20−30 nm size and high specific surface areas of 30−40 m^2/g.[143]

Other SINP Types. The synthesis of pyrrhotite (Fe_7S_8) SINPs (∼30 nm) can be accomplished by mixing iron(III) chloride hexa-hydrate and thiourea in a mixture of ethylene glycol H_2O and autoclaving the mixture at high temperature.[139] Similarly, both nanowires and nanosheets of pyrrhotite can be produced by varying the synthesis conditions and processing of the resultant precipitate.[150,151] A variety of synthesis methods have also been used to generate and stabilize greigite nanocrystals, [152,153] which display excellent sorption capacity and separation properties. Bimetallic FeMoS nanoparticles can be synthesized via thermal

decomposition of iron hteteropolymolybdates, and Fe_7O_8 SINPs, with various morphological properties (i.e., spherical, rods, or plates), can be produced by varying the growth temperature and precursor concentration used.[154]

Greigite, pyyrrhotite, and mixed phase SINPs have also been synthesized using symmetrical- and unsymmetrical-dialkyldithiocarbamatoiron(III) complexes.[36] Aligned cubic phase FeS_{2-x} nanowires can be formed using iron nitrate ($Fe(NO_3)_3 \cdot 9H_2O$) and sodium sulfide (Na_2S),[155] and different nanocrystalline iron sulfides can be produced by reacting $FeSO_4 \cdot 7H_2O$ with Na_2S_3 in toluene simply by changing the reaction temperature and time.[156] High-purity spinel Fe_3S_4 SINPs can be synthesized by dissolving L-cysteine in water and then adding $FeSO_4$.[157]

Mechanical Milling and Alloying. Physical formation of nanosized particulate powder by high-energy milling is referred to as mechanical milling, whereas the milling of a mixture of different metals and compounds has been termed mechanical alloying.[158] In mechanical milling, mechanical energy is applied, typically at room temperature, to stimulate chemical reactions and phase transformations, which would otherwise only occur at elevated temperatures.[159] Ball milling induces multiple forces, occur within microbial cells. The resultant nanoparticles tend to be formed of well-defined crystals with narrow particle-size distributions.[164] Engineered NPs can also be produced by indirect biosynthesis, via redox reactions that occur due to the presence of microbes.

Dissimilatory metal-reducing bacteria, such as *Shewanella*, are of interest because they reduce Fe(III) to Fe(II) species,[127,165] which can then precipitate with sulfide to form biogenic SINPs. *Actinobacter* sp. can also be tuned for extracellular synthesis of SINPs, when reacted with aqueous solutions of ferric chloride−ferrous sulfate.[163] A concentrated bacteria (*S. putrefaciens* CN32) culture can be used for the biosynthesis of FeS SINPs.[165]

Shewanella species can also reduce thiosulfate[127] with *S. oneidensis* MR-1, and gene-modified strains having been used to produce FeS SINPs. The biosynthesis of single domain greigite SINPs by MTB has also been explored,[166,167] but greigite SINP formation occurs under anaerobic conditions and thus requires further downstream processing, which may be too expensive for large-scale SINP synthesis.

Green and Sustainable Synthesis Methods. Recently, various procedures for green NP synthesis have been advanced. Compared to conventional synthesis, green and sustainable synthesis seeks either (i) the use of green materials as synthesis reagents or (ii) the employment of production methods that consume less energy or natural resources.[168] There are various ways of achieving these aims. For example, using natural plant extracts and microbiological materials as reducing, capping, and stabilizing reagents or using ultrasound irradiation to reduce energy and reagent requirements. Such techniques are noted for having lower associated environmental impacts than traditional synthesis techniques.[169,170]

Different biomaterials as stabilizers, including glucose, starch, carboxymethylcellulose (CMC), yeast extract, beef extract, peptone, and gelatin, can be used to form stable FeS SINPs.[171] By using thiourea as a sulfide source, $FeCl_2$ as an iron source, and ethylene glycol as a solvent, the synthesis of pyrite SINPs in a one-pot solvothermal synthesis can be achieved without surfactants, at ambient pressure and relatively low temperature. If the temperature of this synthesis reaction is maintained at boiling point (~180°C) under reflux at atmospheric pressure, pyrite SINPs of ~25 nm will form.[172] For these SINPs, a slight increase of the unit-cell parameter and crystallinity compared to published data for bulk pyrite may result from surface effects.

Another pathway to attain greener and sustainable synthesis of SINPs is by recovering materials from waste streams for reuse. For example, S species such as sulfite and thiosulfate, or their reduction product H_2S, may be harvested from industrial wastewaters. Recovery of

these otherwise wasted chemicals also brings environmental benefits by mitigating a potential source of environmental pollution.[173,174] For example, *Shewanella* bacteria have been exploited to reduce thiosulfate in industrial wastewaters in order to fabricate FeS SINPs, thus achieving both pollution control and SINP biosynthesis.[127]

Thermal reactions have also been developed to prepare green SINPs without the use of hazardous organic solvents or surfactants. For example, mixing ferrocene and elemental S (2.325:1 ratio) and annealing them (without a solvent) at 500°C under an N_2 atmosphere generates an FeS_2 and carbon nanocomposite product.[175]

Other Synthesis Methods and Enhancements. *Chemical Vapor Deposition*. Chemical vapor deposition (CVD) is a well-established method for the preparation of elemental and compound semiconductors, a method that brings the possibility of constituent flux control, in order to adjust stoichiometry. CVD is a means to prepare the epitaxial layers on single crystalline substrates, and in this way, the influence of grain boundaries on photovoltaic (PV) properties can be explored.[176] As one example, highly textured $Fe_{(1+x)}S$ ($0.1 < x < 0.2$) SINPs with rod-like morphology can be deposited on Si by CVD using iron(III) N,N-diethyldithiocarbamate as a single source precursor. Vacuum evaporation of the precursor, followed by thermal decomposition on a silicon substrate, results in the growth of Fe-rich FeS semiconductors.[177]

Magnetron Sputtering and Ion Sputtering. A variety of SINPs have been prepared by magnetron sputtering and ion sputtering. For instance, pyrite SINP with aggregate morphologies can be formed at 400°C by this process using transitional iron sulfides. Pyrite SINPs formed at 460°C have more uniform particle size distributions, and the use of longer annealing time forms crystallite SINPs of more distinguishable structure, with the disappearance of obvious aggregation. The electrical resistivity of pyrite films prepared at both temperatures also increases with increased annealing time.[178]

Ultrasound Irradiation (Sonication). Ultrasound irradiation can be exploited to aid the synthesis of SINPs, wherein the chemical effects are derived from acoustic cavitation formation, growth, and implosive collapse. For instance, pyrite SINPs can be formed in this way, with the ensuing SINPs displaying two phases of pyrite (cubic and marcasite), the average SINP size being ∼29 nm. FT-IR and Raman spectra also suggest the presence of Fe=S, Fe−S, and S−S functional groups.179 Mackinawite-like FeS SINPs and Cu-doped FeS SINPS can be similarly formed using ultrasound irradiation by adjusting the synthesis conditions and postsynthesis treatment procedures.180 Pyrite SINPs can also be synthesized with the aid of ultrasound irradiation by one-step sonication and autoclaving.181

Plasma Processes. The use of nonthermal N_2 plasma processes may be an effective approach for the preparation of SINP materials from natural bulk minerals, owing to the sputtering effect. An example of this method is the adding of crushed pyrite ore (microsized) to a glow discharge plasma reactor. The reactor comprises a horizontal borosilicate tube of N_2 gas with a high voltage direct current supplied via aluminium bonnets. The pyrite SINPs fabricated by this method are in the 30−50 nm size range. The chemical structure of pyrite is not affected by plasma processes, but it should be noted that SINPS formed this way may display irregular rough surfaces.[132]

Subtractive Methods. Subtractive methods can be applied for the formation of various SINPs including the synthesis of FeS_2 nanotubes from iron oxide nanotubes (produced anodically before sulfurization) with S vapor.[182] Other metal oxides nanotubes and porous structures could potentially be converted to sulfide nanotubes and porous sulfides in the same manner. However, optimization of structure retention and phase purity requires further research. Additionally, the advantage of sulfurization with elemental S rather than H_2S needs further consideration.[183]

Template-Directed Synthesis. By using a sol−gel method, highly ordered iron pyrite (FeS_2) nanowires and nanotube arrays can be fabricated using templates composed of materials such as anodic aluminum oxide (AAO).[49] For this procedure, hydrate ferric nitrate solvents are heated while stirring. Nanoporous AAO template tubes (200 nm internal diameter) are then added under negative pressure to ensure the tube spaces are filled before annealing to form nanotubes. If this is repeated three times, nanowires will be formed instead of tubes. Afterward, SINPs are formed by further annealing in a sulphurous atmosphere. Finally, the AAO template is removed using a NaOH solution (Figure 10). The resultant SINP nanowires and nanotubes crystal phase is cubic FeS_2. The nanotubes do not display a clear absorption edge, and the FeS_2 nanowires have direct optical band gaps of 0.98 and 1.23 eV, respectively, indicating suitability for PV applications.

Polyol-Mediated Process. Polyol processes exploit high-boiling polyalcohol solvents such as glycerol, diethylene glycol, ethylene glycol, and tetraethylene glycol, which also function as mild reducing agents. This method was originally developed for the synthesis of nanocrystalline late transition elements (e.g., Pd), but it can be adapted for the synthesis of SINPs.

For the production of greigite SINPs by a polypol-mediated method, $Fe(COOCH_3)_2$ can be used as a cation source, polyvinylpyrrolidone powder as a capping agent, and thiourea as a S source in a diethylene glycol solvent under an Ar atmosphere. If the mixture is refluxed under stirring, a black precipitate of polyvinylpyrrolidone powder-coated Fe_3S_4 SINPs (9−20 nm) form, which can be separated using an external magnetic field. Of these, the smaller-sized SINP particles are nonstoichiometric greigite with a cation vacancy, while the larger SINPs consist of stoichiometric greigite. These SINPs display ferromagnetic behavior from −195 to 27°C with a magnetic moment of ≈3.5 μB per Fe_3S_4 unit.[29] This method is noted for its low reaction temperature and pressure, making it aligned with green synthesis.

Carbon-Supported SINPs. Common to other NPs, SINPs are vulnerable to coalescing into aggregates, owing to their surface energy, van der Waals forces, magnetic attraction, and other interactions. Support materials can reduce the tendency of SINP products to agglomerate. Ideally, the support materials used for environmental applications should (i) be chemically and physically stable, (ii) show strong surface chemical−physical binding with the SINP, (iii) be of high specific surface area, (iv) show good adsorption capacity for any contaminants of concern, if applicable, (v) be favorable for liquid−solid phase separation, and (vi) be amenable to simple reactor designs with low mass transfer limitations.184 Suitable solid support materials can also expand the effective pH range.[185]

Organic C support matrices can potentially match these requirements. Biochar is a recalcitrant form of C produced by the pyrolysis of biomass,[186] which can be used as a support for SINPs. For example, FeS SINPs can attach to biochar surfaces via −OH, C=C,O=C−O, C−O, and Si−O functional groups, providing these SINPs with excellent adsorption and reducing capability. These characteristics make this material suitable for Cr(VI) removal from polluted waters. In one such case, 57% of Cr(VI) removal was attributed to reduction reactions, and the remainder was attributed to adsorption.[121]

Summary and Future Research Directions. Our understanding of SINP formation in the natural environment has been enhanced by studies of submarine hydrothermal vents, as well as studies of SINPs in the lithosphere, microbial processes, and even in outer space. Consequently, we are now aware of some of the key roles SINPs play in many natural systems, and this is of importance for the development of engineered SINP synthesis procedures. For example, the use of H_2S as a sulfur source with SiO_2 allows the synthesis of pyrite particles that are morphologically similar to those observed at hydrothermal vents,[98] exemplifying the potential for nature-based solutions. Moreover, there has been increasing use of nature-based biosynthesis approaches for the fabrication of engineered NPs.

With increasing interest in greener and sustainable practices among the research community,[187,188] traditionally engineered NP synthesis techniques are becoming more of a concern due to their high energy and resource demand and the use of potentially hazardous or environmentally harmful reagents.[189,190] For example, conventional solvothermal synthesis often uses toxic organic solvents. To circumvent this, researchers are developing facile one-step methods that use common laboratory regents. Reducing the environmental impacts of SINP synthesis is particularly significant when the product is used for environmental remediation purposes where the main goal is to protect human health and the environment. Previously, researchers have concentrated on maximizing efficacy and achieving remediation goals, but more holistic approaches in the development of new greener remediation materials are needed for a sustainable future.[191−194]

Research output pertaining to SINP formation has increased dramatically in recent years, but further opportunities need to be identified. There are still challenges to be faced. There are exciting new directions for research on SINPs, including studies involving regeneration or upscaling synthetic protocols to aid the commercialization of SINPs; however, improved green synthesis approaches must be first developed to alleviate concerns regarding some of the more toxic synthesis process presently used.

AUTHOR INFORMATION

Corresponding Authors

Deyi Hou − School of Environment, Tsinghua University, Beijing 100084, China; orcid.org/0000-0002-0511-5806; Email: hou.deyi@tsinghua.edu.cn

Rajender S. Varma − Regional Centre of Advanced Technologies and Materials, Faculty of Science, Palacky University, 783 71 Olomouc, Czech Republic; orcid.org/0000-0001-9731-6228; Email: varma.rajender@epa.gov

Authors

David O'Connor − School of Environment, Tsinghua University, Beijing 100084, China

Qingsong Liu − Department of Ocean Science and Engineering, Southern University of Science and Technology, Shenzhen 518055, China

Martin R. Palmer − School of Ocean and Earth Science, University of Southampton, Southampton SO14 3ZH, United Kingdom

Complete contact information is available at:

https://pubs.acs.org/10.1021/acssuschemeng.0c03401

Author Contributions

The manuscript was written through contributions of all authors. All authors have given approval to the final version of the manuscript.

Notes

The authors declare no competing financial interest.

REFERENCES

(1) ISO/TS 80004−2:2015. Nanotechnologies-Vocabulary-Part 2: Nano-objects; International Organization for Standardization: Geneva, Switzerland, 2015.

(2) Cao, G. Nanostructures and Nanomaterials: Synthesis, Properties and Applications; World Scientific: Singapore, 2004.

(3) Kelly, K. L.; Coronado, E.; Zhao, L. L.; Schatz, G. C. The Optical Properties of Metal Nanoparticles: The Influence of Size, Shape, and Dielectric Environment. J. Phys. Chem. B 2003, 107 (3), 668−677.

(4) Daniel, M. C.; Astruc, D. Gold nanoparticles: assembly, supramolecular chemistry, quantum-size-related properties, and applications toward biology, catalysis, and nanotechnology. Chem. Rev. 2004, 104 (1), 293−346.

(5) Burda, C.; Chen, X.; Narayanan, R.; El-Sayed, M. A. Chemistry and properties of nanocrystals of different shapes. Chem. Rev. 2005, 105 (4), 1025−102.

(6) Duan, J.; Ji, H.; Zhao, X.; Tian, S.; Liu, X.; Liu, W.; Zhao, D. Immobilization of U(VI) by stabilized iron sulfide nanoparticles: Water chemistry effects, mechanisms, and long-term stability. Chem. Eng. J. 2020, 393, 124692.

(7) Wang, M.; Li, Y.; Zhao, D.; Zhuang, L.; Yang, G.; Gong, Y. Immobilization of mercury by iron sulfide nanoparticles alters mercury speciation and microbial methylation in contaminated groundwater. Chem. Eng. J. 2020, 381, 122664.

(8) Lozano, J. G.; Dillon, F.; Naylor, A. J.; Lee, L. Y.; Lippard, C.; Johnstone, D.; Bruce, P. G.; Grobert, N. Single source precursor route to iron sulfide nanomaterials for energy storage. Chem. Phys. Lett. 2020, 739, 136993.

(9) Wu, H.; Liu, J.; Liang, H.; Zang, D. Sandwich-like Fe3O4/Fe3S4 composites for electromagnetic wave absorption. Chem. Eng. J. 2020, 393, 124743.

(10) Rana, A.; Yadav, K.; Jagadevan, S. A comprehensive review on green synthesis of nature-inspired metal nanoparticles: Mechanism, application and toxicity. J. Cleaner Prod. 2020, 272, 122880.

(11) Sharma, V. K.; Filip, J.; Zboril, R.; Varma, R. S. Natural inorganic nanoparticles–formation, fate, and toxicity in the environment. Chem. Soc. Rev. 2015, 44 (23), 8410−23.

(12) Hou, D.; O'Connor, D.; Igalavithana, A. D.; Alessi, D. S.; Luo, J.; Tsang, D. C. W.; Sparks, D. L.; Yamauchi, Y.; Rinklebe, J.; Ok, Y. S. Metal contamination and bioremediation of agricultural soils for food safety and sustainability. Nature Reviews Earth & Environment 2020, 1 (7), 366−381.

(13) Trogadas, P.; Coppens, M.-O. Nature-Inspired Chemical Engineering. In Sustainable Nanoscale Engineering; Szekely, G., Livingston, A., Eds.; Elsevier, 2020; pp 19−31.

(14) Kou, J.; Lu, C.; Wang, J.; Chen, Y.; Xu, Z.; Varma, R. S. Selectivity Enhancement in Heterogeneous Photocatalytic Transformations. Chem. Rev. 2017, 117 (3), 1445−1514.

(15) Song, Y.; Kirkwood, N.; Maksimovic, C.; Zheng, X.; O'Connor, D.; Jin, Y.; Hou, D. Nature based solutions for contaminated land remediation and brownfield redevelopment in cities: A review. Sci. Total Environ. 2019, 663, 568−579.

(16) Chandrawat, G. S.; Tripathi, J.; Sharma, A.; Singh, J.; Tripathi, S.; Chouhan, J. Study of Structural and Optical Properties of FeS2 Nanoparticles Prepared by Polyol Method. J. Nano-Electron. Phys. 2020, 12 (2), 02016-1−02016-3.

(17) Guan, G.; Li, B.; Zhang, W.; Cui, Z.; He, S. A.; Zou, R.; Lu, X.; Hu, J. High-efficiency and safe sulfur-doped iron oxides for magnetic resonance imaging-guided photothermal/magnetic hyperthermia therapy. Dalton Trans 2020, 49 (17), 5493−5502.

(18) Shi, Z.; Jayatissa, A. H. Preparation and characterization of cobalt-doped iron pyrite (FeS2) thin films. Prog. Nat. Sci. 2020, 30 (3), 352−359.

(19) Rickard, D.; Luther, G. W. 3rd, Chemistry of iron sulfides. Chem. Rev. 2007, 107 (2), 514−62.

(20) Posfai, M.; Buseck, P. R.; Bazylinski, D. A.; Frankel, R. B. Iron sulfides from magnetotactic bacteria; structure, composition, and phase transitions. Am. Mineral. 1998, 83 (11-12 Part 2), 1469−1481.

(21) Taylor, L.; Finger, L. Structural Refinement and Composition of Mackinawite. In Carnegie Institute of Washington Geophysical Laboratory Annual Report, 1970; Vol. 69, pp 318−322.

(22) Akhtar, M.; Malik, M. A.; Tuna, F.; O'Brien, P. The synthesis of iron sulfide nanocrystals from tris(O-alkylxanthato)iron(iii) complexes. J. Mater. Chem. A 2013, 1 (31), 8766−8774.

(23) Wang, H.; Salveson, I. A review on the mineral chemistry of the non-stoichiometric iron sulphide, Fe1- x S (0≤ x≤ 0.125): polymorphs, phase relations and transitions, electronic and magnetic structures. Phase Transitions 2005, 78 (7−8), 547−567.

(24) Vaughan, D. J.; Craig, J. R. Mineral Chemistry of Metal Sulfides; Cambridge Earth Science Series; Cambridge University Press, 1978.

(25) Dekkers, M. J. Magnetic properties of natural pyrrhotite. II. High and low-temperature behaviour of Jrs and TRM as function of grain size. Phys. Earth Planet. Inter. 1989, 57 (3−4), 266−283.

(26) Zhang, B.; de Wijs, G. A.; de Groot, R. A. Switchable Fermi surface sheets in greigite. Phys. Rev. B: Condens. Matter Mater. Phys. 2012, 86 (2), 020406.

(27) Skinner, B. J.; Erd, R. C.; Grimaldi, F. S. Greigite, the thio-spinel of iron; a new mineral. Am. Mineral. 1964, 49 (5−6), 543−555.

(28) Uda, M. On the synthesis of greigite. Am. Mineral. 1965, 50, 1487−1489.

(29) Lyubutin, I. S.; Starchikov, S. S.; Lin, C.-R.; Lu, S.-Z.; Shaikh, M. O.; Funtov, K. O.; Dmitrieva, T. V.; Ovchinnikov, S. G.; Edelman, I. S.; Ivantsov, R. Magnetic, structural, and electronic properties of iron sulfide Fe3S4 nanoparticles synthesized by the polyol mediated process. J. Nanopart. Res. 2013, 15 (1), na DOI: 10.1007/s11051-012-1397-0.

(30) Beal, J. H. L.; Prabakar, S.; Gaston, N.; Teh, G. B.; Etchegoin, P. G.; Williams, G.; Tilley, R. D. Synthesis and Comparison of the Magnetic Properties of Iron Sulfide Spinel and Iron Oxide Spinel Nanocrystals. Chem. Mater. 2011, 23 (10), 2514−2517.

(31) Taylor, P. The stereochemistry of iron sulphides – a structural rationale for the crystallization of some metastable phases from aqueous solution. Am. Mineral. 1980, 65 (9−10), 1026−1030.

(32) Jeong, H. Y.; Lee, J. H.; Hayes, K. F. Characterization of synthetic nanocrystalline mackinawite: crystal structure, particle size, and specific surface area. Geochim. Cosmochim. Acta 2008, 72 (2), 493−505.

(33) Horng, C. S.; Roberts, A. P. The low-temperature Besnus magnetic transition: Signals due to monoclinic and hexagonal pyrrhotite. Geochem., Geophys., Geosyst. 2018, 19 (9), 3364−3375.

(34) Horng, C.-S.; Roberts, A. P. Authigenic or detrital origin of pyrrhotite in sediments?: Resolving a paleomagnetic conundrum. Earth Planet. Sci. Lett. 2006, 241 (3−4), 750−762.

(35) Harada, T. Transport Properties of Iron Dichalcogenides FeX2(X = S, Se and Te). J. Phys. Soc. Jpn. 1998, 67 (4), 1352−1358.

(36) Akhtar, M.; Akhter, J.; Malik, M. A.; O'Brien, P.; Tuna, F.; Raftery, J.; Helliwell, M. Deposition of iron sulfide nanocrystals from single source precursors. J. Mater. Chem. 2011, 21 (26), 9737−9745.

(37) Nakazawa, H.; Morimoto, N.; Watanabe, E. Direct observation of metal vacancies by high-resolution electron microscopy. Part I: 4C type pyrrhotite (Fe7S8). Am. Mineral. 1975, 60 (5-6_Part_1), 359−366.

(38) Li, F.; Franzen, H. F. Ordering, incommensuration, and phase transitions in pyrrhotite: Part II: a high-temperature X-ray powder diffraction and thermomagnetic study. J. Solid State Chem. 1996, 126 (1), 108−120.

(39) Yue, G. H.; Yan, P. X.; Fan, X. Y.; Wang, M. X.; Qu, D. M.; Yan, D.; Liu, J. Z. Characterization of the single crystalline iron sulphide nanowire array synthesis by pulsed electrodeposition. J. Appl. Phys. 2006, 100 (12), 124313.

(40) Abdelhady, A. L.; Malik, M. A.; O'Brien, P.; Tuna, F. Nickel and Iron Sulfide Nanoparticles from Thiobiurets. J. Phys. Chem. C 2012, 116 (3), 2253−2259.

(41) Dekkers, M. J.; Passier, H. F.; Schoonen, M. A. A. Magnetic properties of hydrothermally synthesized greigite (Fe3S4)–II. High and low-temperature characteristics. Geophys. J. Int. 2000, 141 (3), 809−819.

(42) Kasama, T.; Pósfai, M.; Chong, R. K.; Finlayson, A. P.; Buseck, P. R.; Frankel, R. B.; Dunin-Borkowski, R. E. Magnetic properties, microstructure, composition, and morphology of greigite nanocrystals in magnetotactic bacteria from electron holography and tomography. Am. Mineral. 2006, 91 (8−9), 1216−1229.

(43) Roberts, A. P.; Chang, L.; Rowan, C. J.; Horng, C.-S.; Florindo, F., Magnetic properties of sedimentary greigite (Fe3S4): An update. Rev. Geophys. 2011, 49 (1), DOI: 10.1029/2010RG000336.

(44) Li, L.; Caban-Acevedo, M.; Girard, S. N.; Jin, S. High-purity iron pyrite (FeS2) nanowires as high-capacity nanostructured cathodes for lithium-ion batteries. Nanoscale 2014, 6 (4), 2112−8.

(45) Chang, L.; Rainford, B. D.; Stewart, J. R.; Ritter, C.; Roberts, A. P.; Tang, Y.; Chen, Q. Magnetic structure of greigite (Fe3S4) probed by neutron powder diffraction and polarized neutron diffraction. J. Geophys. Res. 2009, 114 (B7), na DOI: 10.1029/2008JB006260.

(46) Chang, L.; Roberts, A. P.; Rowan, C. J.; Tang, Y.; Pruner, P.; Chen, Q.; Horng, C.-S. Low-temperature magnetic properties of greigite (Fe3S4). Geochem., Geophys., Geosyst. 2009, 10 (1), No. na.

(47) Chang, L.; Roberts, A. P.; Tang, Y.; Rainford, B. D.; Muxworthy, A. R.; Chen, Q. Fundamental magnetic parameters from pure synthetic greigite (Fe3S4). J. Geophys. Res. 2008, 113 (B6), na DOI: 10.1029/2007JB005502.

(48) Chang, L.; Roberts, A. P.; Muxworthy, A. R.; Tang, Y.; Chen, Q.; Rowan, C. J.; Liu, Q.; Pruner, P. Magnetic characteristics of synthetic pseudo-single-domain and multi-domain greigite (Fe3S4). Geophys. Res. Lett. 2007, 34 (24), na DOI: 10.1029/2007GL032114.

(49) Li, Y.; Han, Z.; Jiang, L.; Su, Z.; Liu, F.; Lai, Y.; Liu, Y. Template directed synthesis of ordered iron pyrite (FeS2) nanowires and nanotubes arrays. J. Sol-Gel Sci. Technol. 2014, 72 (1), 100−105.

(50) Jia, X.; Chen, Z.; Cui, X.; Peng, Y.; Wang, X.; Wang, G.; Wei, F.; Lu, Y. Building robust architectures of carbon and metal oxide nanocrystals toward high-performance anodes for lithium-ion batteries. ACS Nano 2012, 6 (11), 9911−9.

(51) Chang, Y. S.; Savitha, S.; Sadhasivam, S.; Hsu, C. K.; Lin, F. H. Fabrication, characterization, and application of greigite nanoparticles for cancer hyperthermia. J. Colloid Interface Sci. 2011, 363 (1), 314−9.

(52) Li, G.; Zhang, B.; Yu, F.; Novakova, A. A.; Krivenkov, M. S.; Kiseleva, T. Y.; Chang, L.; Rao, J.; Polyakov, A. O.; Blake, G. R.; de Groot, R. A.; Palstra, T. T. M. High-purity Fe3S4 greigite microcrystals for magnetic and electrochemical performance. Chem. Mater. 2014, 26 (20), 5821−5829.

(53) Ding, C.; Yan, Y.; Xiang, D.; Zhang, C.; Xian, Y. Magnetic Fe3S4 nanoparticles with peroxidase-like activity, and their use in a photometric enzymatic glucose assay. Microchim. Acta 2016, 183 (2), 625−631.

(54) Puthussery, J.; Seefeld, S.; Berry, N.; Gibbs, M.; Law, M. Colloidal iron pyrite (FeS2) nanocrystal inks for thin-film photovoltaics. J. Am. Chem. Soc. 2011, 133 (4), 716−719.

(55) Bai, Y.; Yeom, J.; Yang, M.; Cha, S.-H.; Sun, K.; Kotov, N. A. Universal Synthesis of Single-Phase Pyrite FeS2 Nanoparticles, Nanowires, and Nanosheets. J. Phys. Chem. C 2013, 117 (6), 2567−2573.

(56) Ennaoui, A.; Fiechter, S.; Jaegermann, W.; Tributsch, H. Photoelectrochemistry of highly quantum efficient single-crystalline n-FeS2 (Pyrite). J. Electrochem. Soc. 1986, 133 (1), 97−106.

(57) Antonucci, V.; Aricó, A.S.; Giordano, N.; Antonucci, P.L.; Russo, U.; Cocke, D.L.; Crea, F. Photoactive screen-printed pyrite anodes for electrochemical photovoltaic cells. Sol. Cells 1991, 31 (2), 119−141.

(58) Ennaoui, A.; Fiechter, S.; Tributsch, H.; Giersig, M.; Vogel, R.; Weller, H. Photoelectrochemical energy conversion obtained with ultrathin organo-metallic-chemical-vapor-deposition layer of FeS2 (pyrite) on TiO2. J. Electrochem. Soc. 1992, 139 (9), 2514−2518.

(59) Steinhagen, C.; Harvey, T. B.; Stolle, C. J.; Harris, J.; Korgel, B. A. Pyrite Nanocrystal Solar Cells: Promising, or Fool's Gold? J. Phys. Chem. Lett. 2012, 3 (17), 2352−6.

(60) Kinner, T.; Bhandari, K. P.; Bastola, E.; Monahan, B. M.; Haugen, N. O.; Roland, P. J.; Bigioni, T. P.; Ellingson, R. J. Majority Carrier Type Control of Cobalt Iron Sulfide (CoxFe1-xS2) Pyrite Nanocrystals. J. Phys. Chem. C 2016, 120 (10), 5706−5713.

(61) Kaur, G.; Singh, B.; Singh, P.; Kaur, M.; Buttar, K. K.; Singh, K.; Thakur, A.; Bala, R.; Kumar, M.; Kumar, A. Preferentially grown nanostructured iron disulfide (FeS2) for removal of industrial pollutants. RSC Adv. 2016, 6 (101), 99120−99128.

(62) Nakamura, S.; Yamamoto, A. Electrodeposition of pyrite (FeS2) thin films for photovoltaic cells. Sol. Energy Mater. Sol. Cells 2001, 65 (1−4), 79−85.

(63) Takahashi, N.; Nakatani, Y.; Yatomi, T.; Nakamura, T. Growth of single-crystal pyrite films by atmospheric pressure chemical vapour deposition. Chem. Mater. 2003, 15 (9), 1763−1765.

(64) Deditius, A. P.; Utsunomiya, S.; Renock, D.; Ewing, R. C.; Ramana, C. V.; Becker, U.; Kesler, S. E. A proposed new type of arsenian pyrite: Composition, nanostructure and geological significance. Geochim. Cosmochim. Acta 2008, 72 (12), 2919−2933.

(65) Wells, J. D.; Mullens, T. E. Gold-Bearing Arsenian Pyrite Determined by Microprobe Analysis, Cortez and Carlin Gold mines, Nevada. Econ. Geol. Bull. Soc. Econ. Geol. 1973, 68 (2), 187−201.

(66) Kolker, A.; Haack, S. K.; Cannon, W. F.; Westjohn, D.; Kim, M.-J.; Nriagu, J.; Woodruff, L. Arsenic in Southeastern Michigan. In Arsenic in Ground Water; Springer, 2003; pp 281−294.

(67) Dai, Z. R.; Bradley, J. P. Iron-nickel sulfides in anhydrous interplanetary dust particles. Geochim. Cosmochim. Acta 2001, 65 (20), 3601−3612.

(68) Trepka-Bloch, C. Cyclic ore formation of some volcanogenic massive sulfide deposits in the skellefte district, Sweden. Miner. Deposita 1985, 20 (1), 23−29.

(69) Liang, D.; Ma, R.; Jiao, S.; Pang, G.; Feng, S. A facile synthetic approach for copper iron sulfide nanocrystals with enhanced thermoelectric performance. Nanoscale 2012, 4 (20), 6265−8.

(70) Chen, Y.; Xu, S.; Li, Y.; Jacob, R. J.; Kuang, Y.; Liu, B.; Wang, Y.; Pastel, G.; Salamanca-Riba, L. G.; Zachariah, M. R.; Hu, L. FeS2 Nanoparticles Embedded in Reduced Graphene Oxide toward Robust, High-Performance Electrocatalysts. Adv. Energy Mater. 2017, 7 (19), 1700482.

(71) Feng, H.; Si, P.-Z.; Xiao, X.-F.; Jin, C.-H.; Yu, S.-J.; Li, Z.-F.; Ge, H.-L. Large scale synthesis of FeS coated Fe nanoparticles as reusable magnetic photocatalysts. Frontiers of Materials Science 2013, 7 (3), 308−311.

(72) Kim, E. J.; Kim, J. H.; Azad, A. M.; Chang, Y. S. Facile Synthesis and Characterization of Fe/FeS Nanoparticles for Environmental Applications. ACS Appl. Mater. Interfaces 2011, 3 (5), 1457−62.

(73) Hochella, M. F.; Spencer, M. G.; Jones, K. L. Nanotechnology: nature’s gift or scientists’ brainchild? Environ. Sci.: Nano 2015, 2 (2), 114−119.

(74) Noguchi, T.; Nakamura, T.; Kimura, M.; Zolensky, M. E.; Tanaka, M.; Hashimoto, T.; Konno, M.; Nakato, A.; Ogami, T.; Fujimura, A.; Abe, M.; Yada, T.; Mukai, T.; Ueno, M.; Okada, T.; Shirai, K.; Ishibashi, Y.; Okazaki, R. Incipient space weathering observed on the surface of Itokawa dust particles. Science 2011, 333 (6046), 1121−5.

(75) Benning, L. G.; Wilkin, R. T.; Barnes, H. L. Reaction pathways in the Fe-S system below 100°C. Chem. Geol. 2000, 167 (1−2), 25−51.

(76) Hunger, S.; Benning, L. G. Greigite: a true intermediate on the polysulfide pathway to pyrite. Geochem. Trans. 2007, 8, 1.

(77) Maher, B. A.; Thompson, R. Quaternary Climates, Environments and Magnetism.; Cambridge University Press: Cambridge, UK, 1999.

(78) Whitney, J. A.; Stormer, J. C., Jr Igneous sulfides in the Fish Canyon Tuff and the role of sulfur in calc-alkaline magmas. Geology 1983, 11 (2), 99−102.

(79) Peiffer, S.; Behrends, T.; Hellige, K.; Larese-Casanova, P.; Wan, M.; Pollok, K. Pyrite formation and mineral transformation pathways upon sulfidation of ferric hydroxides depend on mineral type and sulfide concentration. Chem. Geol. 2015, 400, 44−55.

(80) Berner, R. A. Sedimentary pyrite formation: An update. Geochim. Cosmochim. Acta 1984, 48 (4), 605−615.

(81) Butler, E. C.; Hayes, K. F. Kinetics of the Transformation of Trichloroethylene and Tetrachloroethylene by Iron Sulfide. Environ. Sci. Technol. 1999, 33 (12), 2021−2027.

(82) Dries, J.; Bastiaens, L.; Springael, D.; Diels, L.; Agathos, S. N. Kinetics of Trichloroethene (TCE) Reduction by Zero-Valent Iron: Effect of Medium Composition. In Groundwater Quality: Natural and Enhanced Restoration of Groundwater Pollution; Thornton, S. F., Oswald, S. E., Eds.; International Association of Hydrological Sciences, 2002; pp 397−402.

(83) Fan, D.; Lan, Y.; Tratnyek, P. G.; Johnson, R. L.; Filip, J.; O'Carroll, D. M.; Nunez Garcia, A.; Agrawal, A. Sulfidation of Iron-Based Materials: A Review of Processes and Implications for Water Treatment and Remediation. Environ. Sci. Technol. 2017, 51 (22), 13070−13085.

(84) Hellige, K.; Pollok, K.; Larese-Casanova, P.; Behrends, T.; Peiffer, S. Pathways of ferrous iron mineral formation upon sulfidation of lepidocrocite surfaces. Geochim. Cosmochim. Acta 2012, 81, 69−81.

(85) Burton, E. D.; Bush, R. T.; Sullivan, L. A.; Hocking, R. K.; Mitchell, D. R.; Johnston, S. G.; Fitzpatrick, R. W.; Raven, M.; McClure, S.; Jang, L. Y. Iron-monosulfide oxidation in natural sediments: resolving microbially mediated S transformations using XANES, electron microscopy, and selective extractions. Environ. Sci. Technol. 2009, 43 (9), 3128−34.

(86) Picard, A.; Gartman, A.; Clarke, D. R.; Girguis, P. R. Sulfate reducing bacteria influence the nucleation and growth of mackinawite and greigite. Geochim. Cosmochim. Acta 2018, 220, 367−384.

(87) Yabusaki, S.; Cantrell, K.; Sass, B.; Steefel, C. Multicomponent reactive transport in an in situ zero-valent iron cell. Environ. Sci. Technol. 2001, 35 (7), 1493−503.

(88) Savage, K. S.; Tingle, T. N.;O'Day, P. A.; Waychunas, G. A.; Bird, D. K. Arsenic speciation in pyrite and secondary weathering phases, Mother Lode Gold District, Tuolumne County, California. Appl. Geochem. 2000, 15 (8), 1219−1244.

(89) Richards, J. P.; Kerrich, R. The Porgera gold mine, Papua New Guinea; magmatic hydrothermal to epithermal evolution of an alkali type precious metal deposit. Econ. Geol. Bull. Soc. Econ. Geol. 1993, 88 (5), 1017−1052.

(90) MacLean, P. J.; Fleet, M. E. Detrital pyrite in the Witwatersrand gold fields of South Africa; evidence from truncated growth banding. Econ. Geol. Bull. Soc. Econ. Geol. 1989, 84 (7), 2008−2011.

(91) Watson, J. H. P.; Cressey, B. A.; Roberts, A. P.; Ellwood, D. C.; Charnock, J. M.; Soper, A. K. Structural and magnetic studies on heavy metal- adsorbing iron sulphide nanoparticles produced by sulphate reducing bacteria. J. Magn. Magn. Mater. 2000, 214 (1−2), 13−30.

(92) Friedrich, M. W.; Finster, K. W. Geochemistry. How sulfur beats iron. Science 2014, 344 (6187), 974−5.

(93) Kim, Y.; Lee, Y.; Roh, Y. Microbial Synthesis of Iron Sulfide (FeS) and Iron Carbonate (FeCO3) Nanoparticles. J. Nanosci. Nanotechnol. 2015, 15 (8), 5794−7.

(94) Watson, J. H. P.; Ellwood, D. C.; Soper, A. K.; Charnock, J. Nanosized strongly-magnetic bacterially-produced iron sulfide materials. J. Magn. Magn. Mater. 1999, 203 (1−3), 69−72.

(95) Bosch, J.; Lee, K. Y.; Jordan, G.; Kim, K. W.; Meckenstock, R. U. Anaerobic, nitrate-dependent oxidation of pyrite nanoparticles by Thiobacillus denitrificans. Environ. Sci. Technol. 2012, 46 (4), 2095−101.

(96) Elderfield, H.; Schultz, A. Mid-Ocean Ridge Hydrothermal Fluxes and the Chemical Composition of the Ocean. Annu. Rev. Earth Planet. Sci. 1996, 24 (1), 191−224.

(97) Yücel, M.; Gartman, A.; Chan, C. S.; Luther, G. W. Hydrothermal vents as a kinetically stable source of iron-sulphide-bearing nanoparticles to the ocean. Nat. Geosci. 2011, 4 (6), 367−371.

(98) Gartman, A.; Luther, G. W. Comparison of pyrite (FeS2) synthesis mechanisms to reproduce natural FeS2 nanoparticles found at hydrothermal vents. Geochim. Cosmochim. Acta 2013, 120, 447−458.

(99) Mottl, M. J.; McConachy, T. F. Chemical processes in buoyant hydrothermal plumes on the East Pacific Rise near 21°N. Geochim. Cosmochim. Acta 1990, 54 (7), 1911−1927.

(100) Gartman, A.; Findlay, A. J.; Luther, G. W. Nanoparticulate pyrite and other nanoparticles are a widespread component of hydrothermal vent black smoker emissions. Chem. Geol. 2014, 366, 32−41.

(101) Fike, D. A.; Grotzinger, J. P. A paired sulfate-pyrite δ34S approach to understanding the evolution of the Ediacaran-Cambrian sulfur cycle. Geochim. Cosmochim. Acta 2008, 72 (11), 2636−2648.

(102) Strauss, H. Geological evolution from isotope proxy signals – sulphur. Chem. Geol. 1999, 161 (1−3), 89−101.

(103) Goodfellow, W. D.; Jonasson, I. R. Ocean stagnation and ventilation defined by δ34S secular trends in pyrite and Barite, Selwyn Basin, Yukon. Geology 1984, 12 (10), 583−586.

(104) Roberts, A. P.; Reynolds, R. L.; Verosub, K. L.; Adam, D. P. Environmental magnetic implications of Greigite (Fe3S4) Formation in a 3 m.y. lake sediment record from Butte Valley, northern California. Geophys. Res. Lett. 1996, 23 (20), 2859−2862.

(105) Rowan, C. J.; Roberts, A. P. Magnetite dissolution, diachronous greigite formation, and secondary magnetizations from pyrite oxidation: Unravelling complex magnetizations in Neogene marine sediments from New Zealand. Earth Planet. Sci. Lett. 2006, 241 (1−2), 119−137.

(106) Snowball, I.; Thompson, R. A stable chemical remanence in Holocene sediments. J. Geophys. Res. 1990, 95 (B4), 4471−4479.

(107) Duan, Z.; Liu, Q.; Gai, C.; Zhao, X. Magnetostratigraphic and environmental implications of greigite (Fe3S4) formation from Hole U1433A of the IODP Expedition 349, South China Sea. Mar. Geol. 2017, 394, 82−97.

(108) Liu, J.; Liu, Q.; Zhang, X.; Liu, J.; Wu, Z.; Mei, X.; Shi, X.; Zhao, Q. Magnetostratigraphy of a long Quaternary sediment core in the South Yellow Sea. Quat. Sci. Rev. 2016, 144, 1−15.

(109) Morse, J. W.; Luther, G. W. Chemical influences on trace metal sulfide interactions in anoxic sediments. Geochim. Cosmochim. Acta 1999, 63 (19−20), 3373−3378.

(110) Rosenthal, Y.; Lam, P.; Boyle, E. A.; Thomson, J. Authigenic cadmium enrichments in suboxic sediments: Precipitation and post depositional mobility. Earth Planet. Sci. Lett. 1995, 132 (1−4), 99−111.

(111) Schippers, A.; Jørgensen, B. B. Biogeochemistry of pyrite and iron sulfide oxidation in marine sediments. Geochim. Cosmochim. Acta 2002, 66 (1), 85−92.

(112) Rimstidt, J. D.; Vaughan, D. J. Pyrite oxidation: a state-of-the-art assessment of the reaction mechanism. Geochim. Cosmochim. Acta 2003, 67 (5), 873−880.

(113) Moses, C. O.; Nordstrom, D. K.; Herman, J. S.; Mills, A. L. Aqueous pyrite oxidation by dissolved oxygen and by ferric iron. Geochim. Cosmochim. Acta 1987, 51 (6), 1561−1571.

(114) Singer, P. C.; Stumm, W. Acidic mine drainage: the rate determining step. Science 1970, 167 (3921), 1121−3.

(115) Schwientek, M.; Einsiedl, F.; Stichler, W.; Stögbauer, A.; Strauss, H.; Maloszewski, P. Evidence for denitrification regulated by pyrite oxidation in a heterogeneous porous groundwater system. Chem. Geol. 2008, 255 (1−2), 60−67.

(116) Zhang, Z. J.; Chen, X. Y. Magnetic greigite (Fe3S4) nanomaterials: Shape-controlled solvothermal synthesis and their calcination conversion into hematite (α-Fe2O3) nanomaterials. J. Alloys Compd. 2009, 488 (1), 339−345.

(117) Dwivedi, A. D.; Dubey, S. P.; Sillanpää, M.; Kwon, Y.-N.; Lee, C.; Varma, R. S. Fate of engineered nanoparticles: Implications in the environment. Coord. Chem. Rev. 2015, 287, 64−78.

(118) Cheng, D.; Yuan, S.; Liao, P.; Zhang, P. Oxidizing Impact Induced by Mackinawite (FeS) Nanoparticles at Oxic Conditions due to Production of Hydroxyl Radicals. Environ. Sci. Technol. 2016, 50 (21), 11646−11653.

(119) Lauretta, D. S.; Lodders, K.; Fegley, B., Jr. Experimental simulations of sulfide formation in the solar nebula. Science 1997, 277 (5324), 358−60.

(120) Zolensky, M. E.; Thomas, K. L. Iron and iron-nickel sulfides in chondritic interplanetary dust particles. Geochim. Cosmochim. Acta 1995, 59 (22), 4707−4712.

(121) Lyu, H.; Tang, J.; Huang, Y.; Gai, L.; Zeng, E. Y.; Liber, K.; Gong, Y. Removal of hexavalent chromium from aqueous solutions by a novel biochar supported nanoscale iron sulfide composite. Chem. Eng. J. 2017, 322, 516−524.

(122) Yang, L.; Gao, J.; Liu, Y.; Zhang, Z.; Zou, M.; Liao, Q.; Shang, J. Removal of Methyl Orange from Water Using Sulfur-Modified nZVI Supported on Biochar Composite. Water, Air, Soil Pollut. 2018, 229 (11), na DOI: 10.1007/s11270-018-3992-x.

(123) Gong, Y.; Liu, Y.; Xiong, Z.; Zhao, D. Immobilization of mercury by carboxymethyl cellulose stabilized iron sulfide nanoparticles: reaction mechanisms and effects of stabilizer and water chemistry. Environ. Sci. Technol. 2014, 48 (7), 3986−94.

(124) Esmaili, H.; Kotobi, A.; Sheibani, S.; Rashchi, F. Photocatalytic degradation of methylene blue by nanostructured Fe/FeS powder under visible light. Int. J. Miner., Metall. Mater. 2018, 25 (2), 244−252.

(125) Wang, X.; Cai, W.; Wang, G.; Wu, Z.; Zhao, H. One-step fabrication of high performance micro/nanostructured Fe3S4-C magnetic adsorbent with easy recovery and regeneration properties. CrystEngComm 2013, 15 (15), 2956−2965.

(126) Liu, Y.; Xiao, W.; Wang, J.; Mirza, Z. A.; Wang, T. Optimized Synthesis of FeS Nanoparticles with a High Cr(VI) Removal Capability. J. Nanomater. 2016, 2016, 1.

(127) Xiao, X.; Zhu, W.-W.; Yuan, H.; Li, W.-W.; Li, Q.; Yu, H.-Q. Biosynthesis of FeS nanoparticles from contaminant degradation in one single system. Biochem. Eng. J. 2016, 105, 214−219.

(128) Zhang, Q.; Guo, W.; Yue, X.; Liu, Z.; Li, X. Degradation of Rhodamine B Using FeS-Coated Zero-Valent Iron Nanoparticles in the Presence of Dissolved Oxygen. Environ. Prog. Sustainable Energy 2016, 35 (6), 1673−1678.

(129) Paknikar, K. M.; Nagpal, V.; Pethkar, A. V.; Rajwade, J. M. Degradation of lindane from aqueous solutions using iron sulphide nanoparticles stabilized by biopolymers. Sci. Technol. Adv. Mater. 2005, 6 (3−4), 370−374.

(130) Dutta, A. K.; Maji, S. K.; Srivastava, D. N.; Mondal, A.; Biswas, P.; Paul, P.; Adhikary, B. Synthesis of FeS and FeSe nanoparticles from a single source precursor: a study of their photocatalytic activity, peroxidase-like behavior, and electrochemical sensing of H2O2. ACS Appl. Mater. Interfaces 2012, 4 (4), 1919−1927.

(131) Fathinia, S.; Fathinia, M.; Rahmani, A. A.; Khataee, A. Preparation of natural pyrite nanoparticles by high energy planetary ball milling as a nanocatalyst for heterogeneous Fenton process. Appl. Surf. Sci. 2015, 327, 190−200.

(132) Khataee, A.; Gholami, P.; Vahid, B. Heterogeneous sono-Fenton-like process using nanostructured pyrite prepared by Ar glow discharge plasma for treatment of a textile dye. Ultrason. Sonochem. 2016, 29, 213−225.

(133) Khataee, A.; Gholami, P.; Sheydaei, M.; Khorram, S.; Joo, S. W. Preparation of nanostructured pyrite with N-2 glow discharge plasma and the study of its catalytic performance in the heterogeneous Fenton process. New J. Chem. 2016, 40 (6), 5221−5230.

(134) Khabbaz, M.; Entezari, M. H. Degradation of Diclofenac by sono synthesis of pyrite nanoparticles. J. Environ. Manage. 2017, 187, 416−423.

(135) Gil-Lozano, C.; Losa-Adams, E.; F.-Davila, A.; Gago-Duport, L. Pyrite nanoparticles as a Fenton-like reagent for in situ remediation of organic pollutants. Beilstein J. Nanotechnol. 2014, 5, 855−864.

(136) Ito, D.; Miura, K.; Ichimura, T.; Ihara, I.; Watanabe, T. Removal of As, Cd, Hg and Pb ions from solution by adsorption with bacterially produced magnetic iron sulfide particles using high gradient magnetic separation. IEEE Trans. Appl. Supercond. 2004, 14 (2), 1551−1553.

(137) Su, Y. M.; Adeleye, A. S.; Keller, A. A.; Huang, Y. X.; Dai, C. M.; Zhou, X. F.; Zhang, Y. L. Magnetic sulfide-modified nanoscale zerovalent iron (S-nZVI) for dissolved metal ion removal. Water Res. 2015, 74, 47−57.

(138) Yang, Y.; Chen, T.; Morrison, L.; Gerrity, S.; Collins, G.; Porca, E.; Li, R.; Zhan, X. Nanostructured pyrrhotite supports autotrophic denitrification for simultaneous nitrogen and phosphorus removal from secondary effluents. Chem. Eng. J. 2017, 328, 511−518.

(139) Cantu, J.; Gonzalez, L. E.; Goodship, J.; Contreras, M.; Joseph, M.; Garza, C.; Eubanks, T. M.; Parsons, J. G. Removal of arsenic from water using synthetic Fe7S8 nanoparticles. Chem. Eng. J. 2016, 290, 428−437.

(140) Su, Y. M.; Adeleye, A. S.; Huang, Y. X.; Zhou, X. F.; Keller, A. A.; Zhang, Y. L. Direct Synthesis of Novel and Reactive Sulfide-modified Nano Iron through Nanoparticle Seeding for Improved Cadmium-Contaminated Water Treatment. Sci. Rep. 2016, 6, 13.

(141) Song, S. K.; Su, M. M.; Adeleye, A. S.; Zhang, Y. L.; Zhou, X. F. Optimal design and characterization of sulfide-modified nanoscale zerovalent iron for diclofenac removal. Appl. Catal., B 2017, 201, 211−220.

(142) Sinha, S.; Amy, G.; Yoon, Y.-M.; Her, N.-G. Arsenic Removal from Water Using Various Adsorbents: Magnetic Ion Exchange Resins, Hydrous Ion Oxide Particles, Granular Ferric Hydroxide, Activated Alumina, Sulfur Modified Iron, and Iron Oxide-Coated Microsand. Environ. Eng. Res. 2011, 16 (3), 165−173.

(143) Kim, E.-J.; Kim, J.-H.; Azad, A.-M.; Chang, Y.-S. Facile Synthesis and Characterization of Fe/FeS Nanoparticles for Environmental Applications. ACS Appl. Mater. Interfaces 2011, 3 (5), 1457−1462.

(144) de Carvalho, L. M.; Schwedt, G. Polarographic determination of dithionite and its decomposition products: kinetic aspects, stabilizers, and analytical application. Anal. Chim. Acta 2001, 436 (2), 293−300.

(145) Meester, B.; Reijnen, L.; Goossens, A.; Schoonman, J. Synthesis of Pyrite (FeS2) Thin Films by Low-Pressure MOCVD. Chem. Vap. Deposition 2000, 6 (3), 121−128.

(146) Xuefeng, Q.; Yi, X.; Yitai, Q. Solventothermal synthesis and morphological control of nanocrystalline FeS2. Mater. Lett. 2001, 48 (2), 109−111.

(147) Wu, R.; Zheng, Y. F.; Zhang, X. G.; Sun, Y. F.; Xu, J. B.; Jian, J. K. Hydrothermal synthesis and crystal structure of pyrite. J. Cryst. Growth 2004, 266 (4), 523−527.

(148) Liu, J.; Wen, Y.; Wang, Y.; Van Aken, P. A.; Maier, J.; Yu, Y. Carbon-Encapsulated Pyrite as Stable and Earth-Abundant High Energy Cathode Material for Rechargeable Lithium Batteries. Adv. Mater. 2014, 26 (34), 6025−6030.

(149) Malek, T. J.; Chaki, S. H.; Deshpande, M. P. Structural, morphological, optical, thermal and magnetic study of mackinawite FeS nanoparticles synthesized by wet chemical reduction technique. Phys. B 2018, 546, 59−66.

(150) Nath, M.; Choudhury, A.; Kundu, A.; Rao, C. N. R. Synthesis and characterization of magnetic iron sulfide nanowires. Adv. Mater. 2003, 15 (24), 2098−2101.

(151) Han, W.; Gao, M. Y. Investigations on iron sulfide nano sheets prepared via a single-source precursor approach. Cryst. Growth Des. 2008, 8 (3), 1023−1030.

(152) Vanitha, P.; O'Brien, P. Phase Control in the Synthesis of Magnetic Iron Sulfide Nanocrystals From a Cubane-Type Fe- S Cluster. J. Am. Chem. Soc. 2008, 130 (51), 17256−17257.

(153) Escalona, E. E.; Pereira-Almao, P. R.; Castillo, J.; Hung, J.; Bolivar, C.; Scott, C. E. Nanometric bimetallic sulfides prepared via thermal decomposition of Ni and Fe hetero polymolybdate emulsions. Catal. Lett. 2006, 112 (3−4), 227−230.

(154) Abdelhady, A. L.; Malik, M. A.;O'Brien, P.; Tuna, F. Nickel and Iron Sulfide Nanoparticles from Thiobiurets. J. Phys. Chem. C 2012, 116 (3), 2253−2259.

(155) Kar, S.; Chaudhuri, S. Synthesis of highly oriented iron sulphide nanowires through solvo thermal process. Mater. Lett. 2005, 59 (2−3), 289−292.

(156) Qian, X.F.; Zhang, X.M.; Wang, C.; Xie, Y.; Wang, W.Z.; Qian, Y.T. The preparation and phase transition of nanocrystalline iron sulfides via toluene-thermal process. Mater. Sci. Eng., B 1999, 64 (3), 170−173.

(157) Li, P.; Xia, C.; Zhang, Q.; Guo, Z.; Cui, W.; Bai, H.; Alshareef, H. N.; Zhang, X.-x. Fabrication and characterization of nanostructured Fe3S4, an isostructural compound of half-metallic Fe3O4. J. Appl. Phys. 2015, 117 (22), 223903.

(158) Suryanarayana, C. Mechanical Alloying: A Novel Technique to Synthesize Advanced Materials. Prog. Mater. Sci. 2001, 46 (1−2), 1−184.

(159) Baláž, P.; Boldižárová, E.; Godočíková, E.; Briančin, J. Mechanochemical route for sulphide nanoparticles preparation. Mater. Lett. 2003, 57 (9−10), 1585−1589.

(160) Chin, P. P.; Ding, J.; Yi, J. B.; Liu, B. H. Synthesis of FeS2 and FeS nanoparticles by high-energy mechanical milling and mechanochemical processing. J. Alloys Compd. 2005, 390 (1−2), 255−260.

(161) Khataee, A.; Fathinia, S.; Fathinia, M. Production of pyrite nanoparticles using high energy planetary ball milling for sono catalytic degradation of sulfasalazine. Ultrason. Sonochem. 2017, 34, 904−915.

(162) Balaz, P.; Dutkova, E.; Skorvanek, I.; Gock, E.; Kovac, J.; Satka, A. Kinetics of mechanochemical synthesis of Me/FeS (Me = Cu, Pb, Sb) nanoparticles. J. Alloys Compd. 2009, 483 (1−2), 484−487.

(163) Bharde, A. A.; Parikh, R. Y.; Baidakova, M.; Jouen, S.; Hannoyer, B.; Enoki, T.; Prasad, B. L. V.; Shouche, Y. S.; Ogale, S.; Sastry, M. Bacteria-mediated precursor-dependent biosynthesis of superparamagnetic iron oxide and iron sulfide nanoparticles. Langmuir 2008, 24 (11), 5787−5794.

(164) Sharma, V. K.; Filip, J.; Zboril, R.; Varma, R. S. Natural inorganic nanoparticles-formation, fate, and toxicity in the environment. Chem. Soc. Rev. 2015, 44 (23), 8410−8423.

(165) Huo, Y.-C.; Li, W.-W.; Chen, C.-B.; Li, C.-X.; Zeng, R.; Lau, T.-C.; Huang, T.-Y. Biogenic FeS accelerates reductive dechlorination of carbon tetrachloride by Shewanella putrefaciens CN32. Enzyme Microb. Technol. 2016, 95, 236−241.

(166) Farina, M.; Esquivel, D. M. S.; De Barros, H. G. P. L. Magnetic iron-sulphur crystals from a magnetotactic microorganism. Nature 1990, 343 (6255), 256−258.

(167) Mann, S.; Sparks, N. H. C.; Frankel, R. B.; Bazylinski, D. A.; Jannasch, H. W. Biomineralization of ferrimagnetic greigite (Fe3S4) and iron pyrite (FeS2) in a magnetotactic bacterium. Nature 1990, 343 (6255), 258−261.

(168) Wang, Y.;O'Connor, D.; Shen, Z.; Lo, I. M. C.; Tsang, D. C. W.; Pehkonen, S.; Pu, S.; Hou, D. Green synthesis of nanoparticles for the remediation of contaminated waters and soils: Constituents, synthesizing methods, and influencing factors. J. Cleaner Prod. 2019, 226, 540−549.

(169) Seo, H.; Roh, Y. Mixed Contaminants Removal Efficiency Using Bio-FeS Nanoparticles. J. Nanosci. Nanotechnol. 2018, 18 (2), 1127−1130.

(170) Hou, D. Sustainable Remediation of Contaminated Soil and Groundwater: Materials, Processes, and Assessment; Butterworth-Heinemann: Oxford, U.K., 2019.

(171) Shao, D.; Ren, X.; Wen, J.; Hu, S.; Xiong, J.; Jiang, T.; Wang, X.; Wang, X. Immobilization of uranium by biomaterial stabilized FeS nanoparticles: Effects of stabilizer and enrichment mechanism. J. Hazard. Mater. 2016, 302, 1−9.

(172) Giaccherini, A.; Colantoni, I.; D'Acapito, F.; De Luca, A.; Capolupo, F.; Montegrossi, G.; Romanelli, M.; Innocenti, M.; Di Benedetto, F. Green synthesis of pyrite nanoparticles for energy conversion and storage: a spectroscopic investigation. Eur. J. Mineral. 2016, 28 (3), 611−618.

(173) Lens, P. N. L.; Visser, A.; Janssen, A. J. H.; Pol, L.W. H.; Lettinga, G. Biotechnological treatment of sulfate-rich wastewaters. Crit. Rev. Environ. Sci. Technol. 1998, 28 (1), 41−88.

(174) Meulepas, R. J. W.; Jagersma, C. G.; Khadem, A. F.; Buisman, C. J. N.; Stams, A. J. M.; Lens, P. N. L. Effect of environmental conditions on sulfate reduction with methane as electron donor by an Eckernförde Bay enrichment. Environ. Sci. Technol. 2009, 43 (17), 6553−6559.

(175) Fei, L.; Jiang, Y. F.; Xu, Y.; Chen, G.; Li, Y. L.; Xu, X.; Deng, S. G.; Luo, H. M. A novel solvent-free thermal reaction of ferrocene and sulfur for one-step synthesis of iron sulfide and carbon nanocomposites and their electrochemical performance. J. Power Sources 2014, 265, 1−5.

(176) Bronold, M.; Kubala, S.; Pettenkofer, C.; Jaegermann, W. Thin pyrite (FeS2) films by molecular beam deposition. Thin Solid Films 1997, 304 (1−2), 178−182.

(177) Soon, J. M.; Goh, L. Y.; Loh, K. P.; Foo, Y. L.; Ming, L.; Ding, J. Highly textured, magnetic Fe (1+ x) S nanorods grown on silicon. Appl. Phys. Lett. 2007, 91 (8), 084105.

(178) Meng, L.; Liu, Y. H.; Tian, L. Structural, optical and electrical properties of polycrystalline pyrite (FeS2) films obtained by thermal sulfuration of iron films. J. Cryst. Growth 2003, 253 (1−4), 530−538.

(179) Khabbaz, M.; Entezari, M. H. Simple and versatile one-step synthesis of FeS2 nanoparticles by ultrasonic irradiation. J. Colloid Interface Sci. 2016, 470, 204−210.

(180) Zavašnik, J.; Stanković, N.; Arshad, S. M.; Rečnik, A. Sonochemical synthesis of mackinawite and the role of Cu addition on phase transformations in the Fe-S system. J. Nanopart. Res. 2014, 16 (2), na DOI: 10.1007/s11051-013-2223-z.

(181) Guo, C.; Tong, X.; Guo, X.-y. Solvothermal synthesis of FeS2 nanoparticles for photoelectrochemical hydrogen generation in neutral water. Mater. Lett. 2015, 161, 220−223.

(182) Shi, Z.; Fan, D.; Johnson, R. L.; Tratnyek, P. G.; Nurmi, J. T.; Wu, Y.; Williams, K. H. Methods for characterizing the fate and effects of nano zerovalent iron during groundwater remediation. J. Contam. Hydrol. 2015, 181, 17−35.

(183) Kolasinski, K. W. Subtractive methods to form pyrite and sulphide nanostructures of Fe, Co, Ni, Cu and Zn. Curr. Opin. Solid State Mater. Sci. 2016, 20 (6), 371−373.

(184) Sharma, S.; Pollet, B. G. Support materials for PEMFC and DMFC electrocatalysts – A review. J. Power Sources 2012, 208, 96−119.

(185) Zhang, P.; Lo, I.; O'Connor, D.; Pehkonen, S.; Cheng, H.; Hou, D. High efficiency removal of methylene blue using SDS surface modified ZnFe2O4 nanoparticles. J. Colloid Interface Sci. 2017, 508, 39−48.

(186) Wang, L.; Ok, Y. S.; Tsang, D. C. W.; Alessi, D. S.; Rinklebe, J.; Wang, H.; Masek, O.; Hou, R.; O'Connor, D.; Hou, D. New trends in biochar pyrolysis and modification strategies: feedstock, pyrolysis conditions, sustainability concerns and implications for soil amendment. Soil Use Manage. 2020, 36 (3), 358−386.

(187) O'Connor, D.; Hou, D. Targeting Cleanups Towards a More Sustainable Future. Environmental Science: Processes & Impacts 2018, 20, 266.

(188) Hou, D. Sustainable Remediation of Contaminated Soil and Groundwater: Materials, Processes, and Assessment; Butterworth-Heinemann: Oxford, U.K., 2020.

(189) Kalaiselvi, A.; Roopan, S. M.; Madhumitha, G.; Ramalingam, C.; Elango, G. Synthesis and characterization of palladium nanoparticles using Catharanthus roseus leaf extract and its application in the photocatalytic degradation. Spectrochim. Acta, Part A 2015, 135, 116−9.

(190) Yang, H.; Liu, X.; Sun, S.; Nie, Y.; Wu, H.; Yang, T.; Zheng, S.; Lin, S. Green and facile synthesis of graphene nanosheets/K3PW12O40 nanocomposites with enhanced photocatalytic activities. Mater. Res. Bull. 2016, 78, 112−118.

(191) O’Connor, D.; Peng, T.; Li, G.; Wang, S.; Duan, L.; Mulder, J.; Cornelissen, G.; Cheng, Z.; Yang, S.; Hou, D. Sulfur-modified rice husk biochar: A green method for the remediation of mercury contaminated soil. Sci. Total Environ. 2018, 621, 819.

(192) Pati, P.; McGinnis, S.; Vikesland, P. J. Life Cycle Assessment of “green” Nanoparticle Synthesis Methods. Environ. Eng. Sci. 2014, 31 (7), 410−420.

(193) Varma, R. S. Greener approach to nanomaterials and their sustainable applications. Curr. Opin. Chem. Eng. 2012, 1 (2), 123−128.

(194) Zhang, P.; O’Connor, D.; Wang, Y.; Jiang, L.; Xia, T.; Wang, L.; Tsang, D. C. W.; Ok, Y. S.; Hou, D. A green biochar/iron oxide composite for methylene blue removal. J. Hazard. Mater. 2020, 384, 121286.

Figures

Figure 1. Heating-induced transition of the magnetic moment configuration in troilite (adapted from Wang and Salveson[23] with permission).

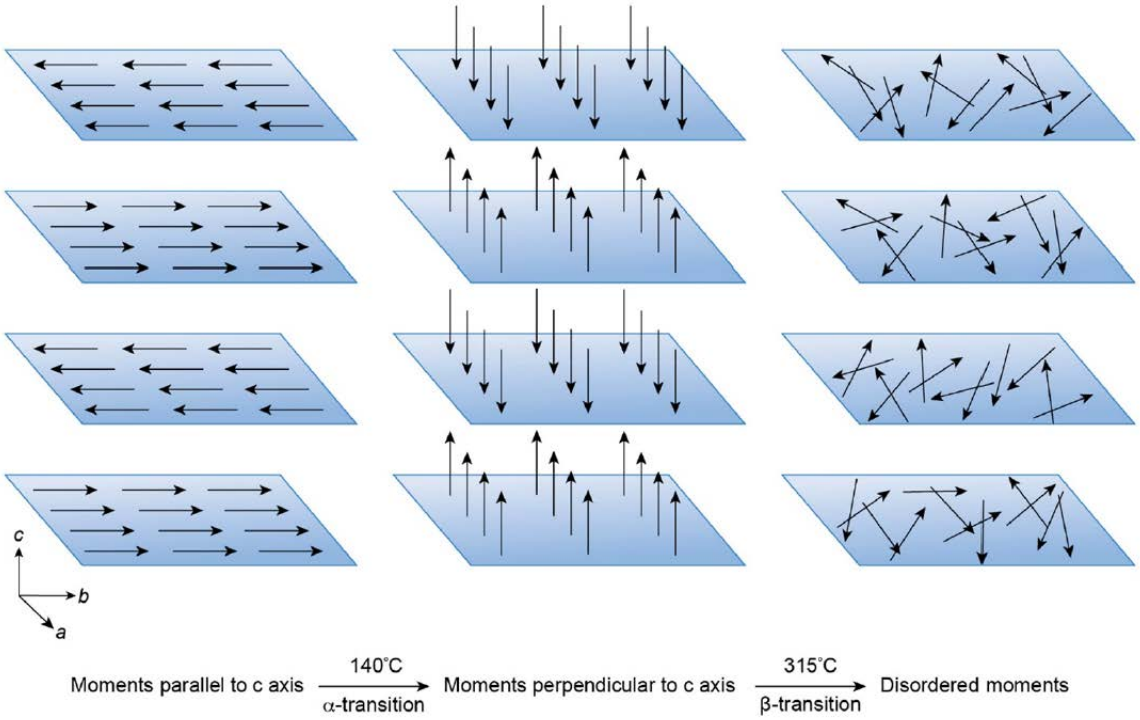

Figure 2. Pathway to pyrite formation (adapted from Berner[80] with permission).

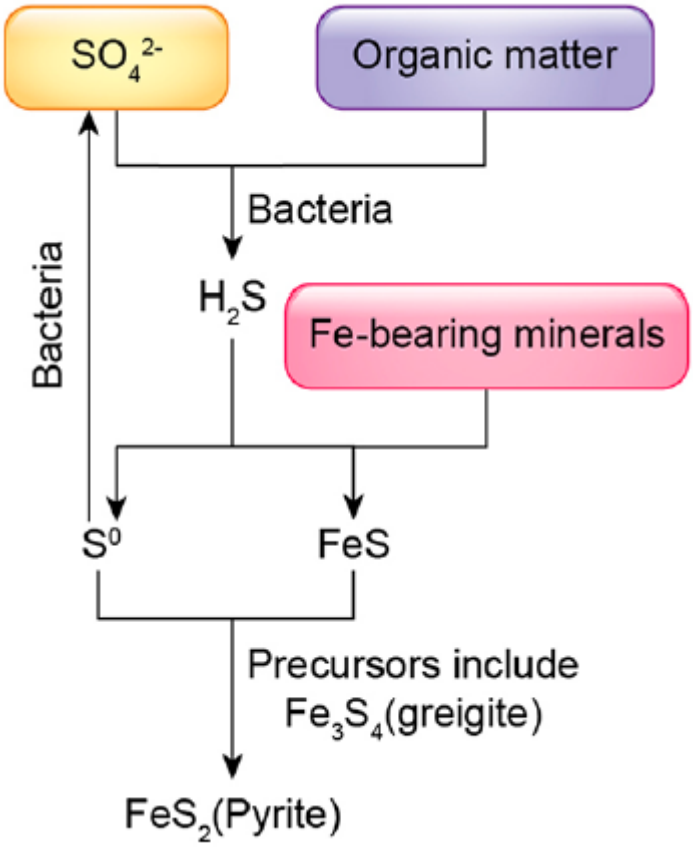

Figure 3. Transmission electron microscopy (TEM) image of the cell of a sulfate-reducing bacterium (SRB) coated with nanosized iron sulfide precipitates (reproduced from Watson et al.[91] with permission).

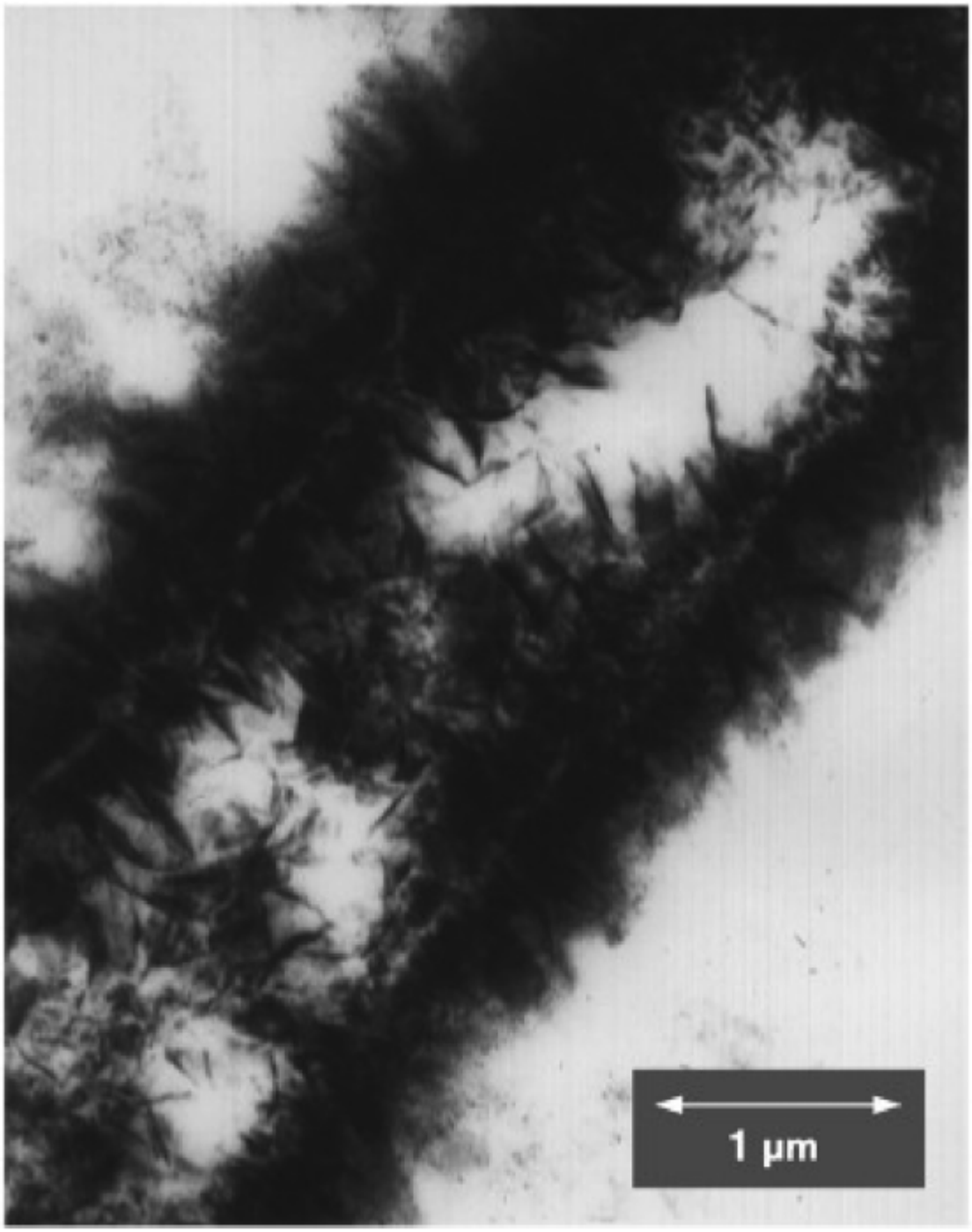

Figure 4. Dissimilatory metal-reducing bacteria can respire elemental sulfur (S^0) as an alternative electron acceptor in alkaline pH aquifer environments leading to mackinawite formation. Microbial (green) and abiotic processes (black) are coupled together (adapted from Friedrich and Finster[92] with permission).

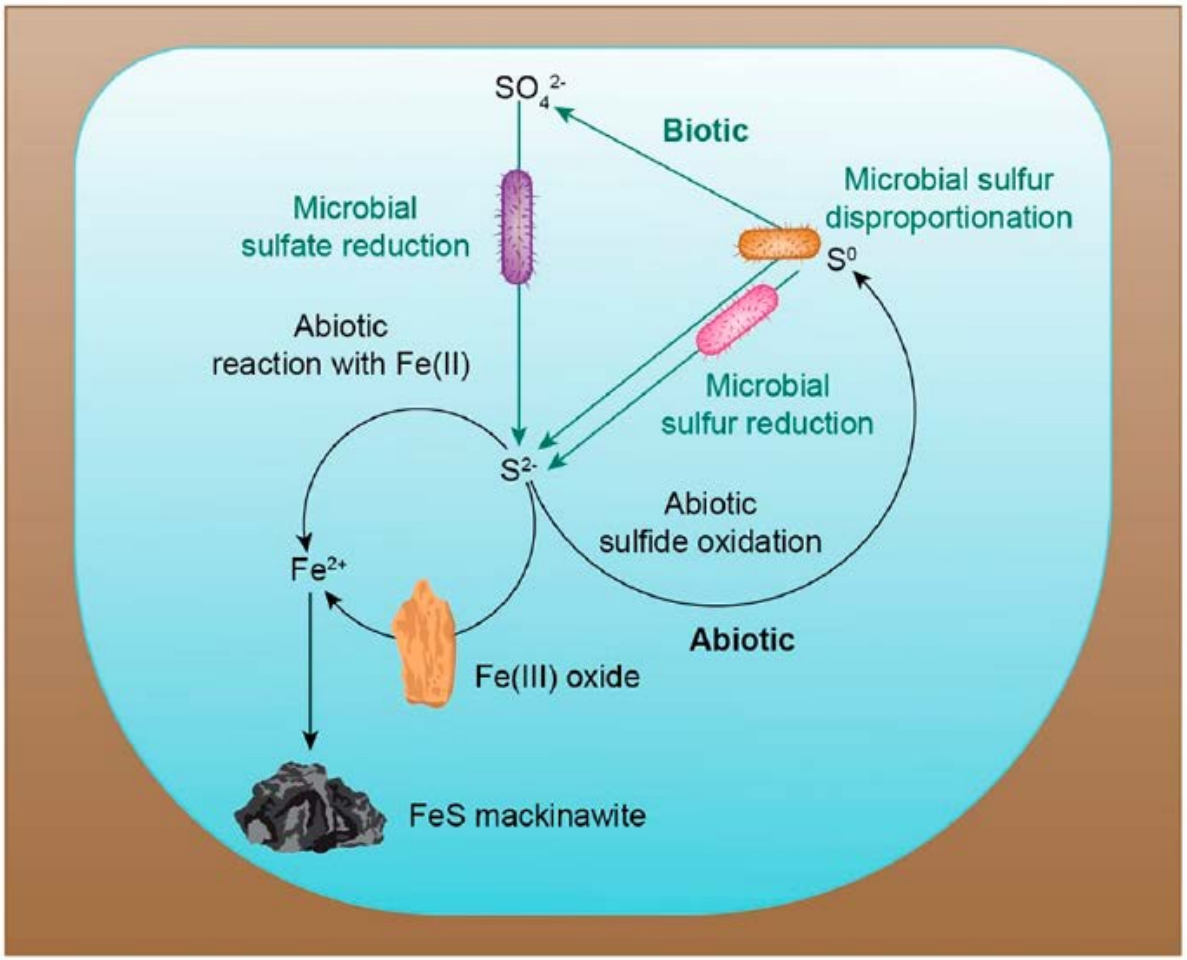

Figure 5. Formation of pyrite SINPs in deep ocean hydrothermal environments. Vent iron may exist in various forms including pyrite (FeS_2) SINPs. By remaining in suspension, pyrite SINPs are able to evade mass precipitation zones rising 1−5 m above hydrothermal vents (adapted from Yücel et al.[97] with permission).

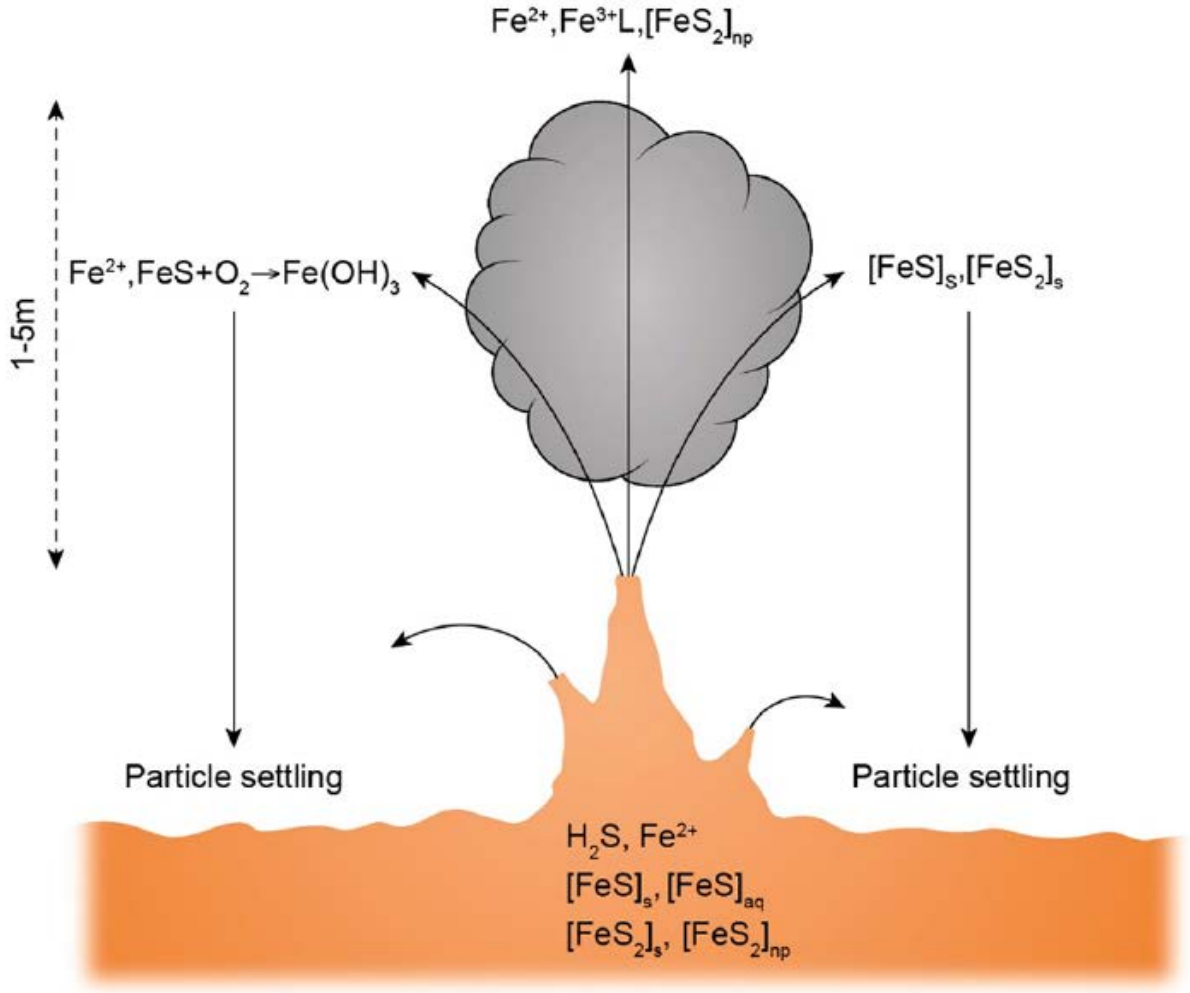

Figure 6. Fe−S system phase diagram showing iron sulfide transition from FeS to FeS_2 at different temperatures (25−1200 °C) (reproduced from Wang and Salveson[23] with permission).

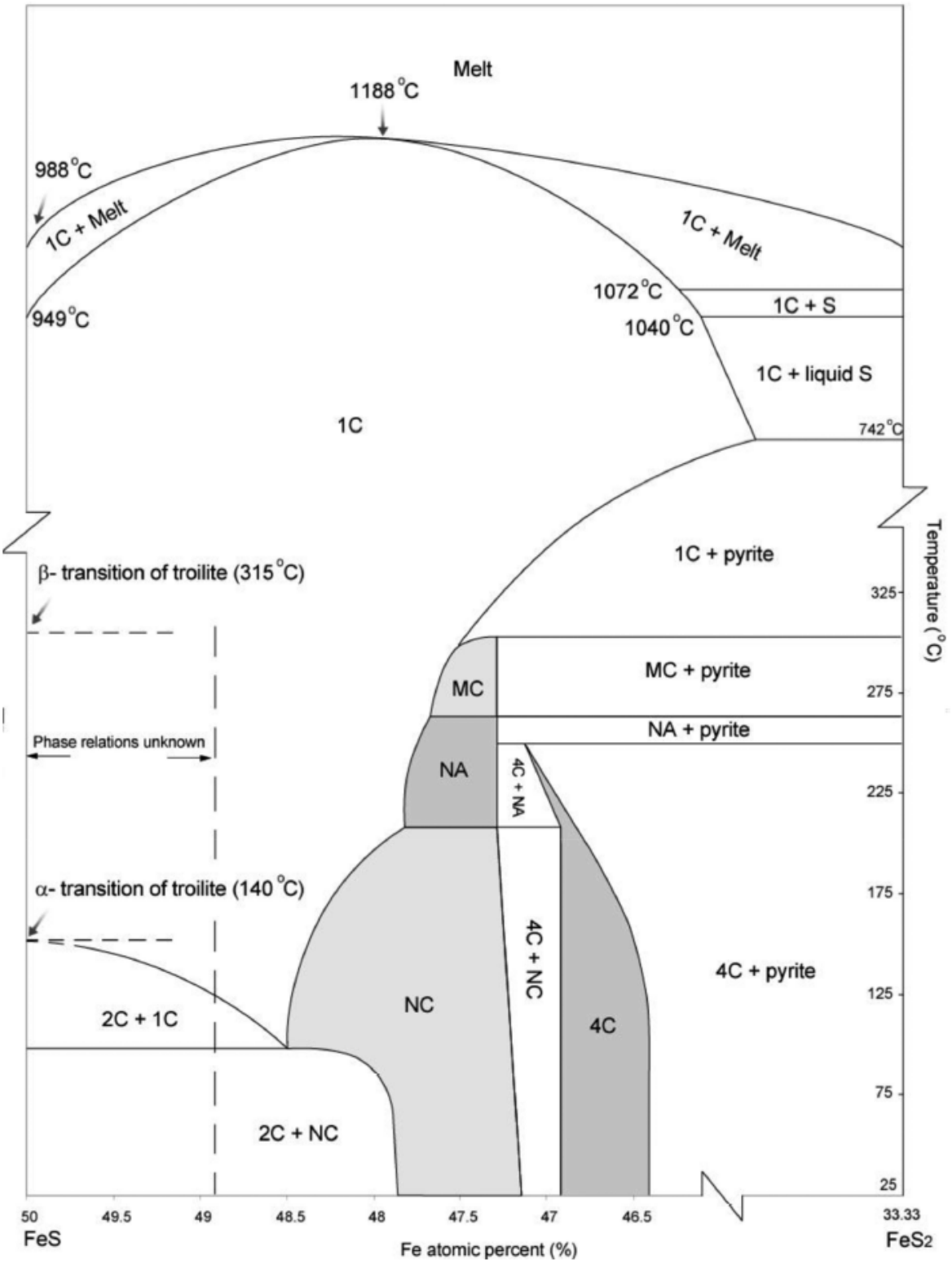

Figure 7. Different FeS_2 SINP morphologies resulting from the use of different solvothermal solvents: (a) ethylenediamine solvent and (b) benzene solvent (reproduced from Xuefeng et al.[146] with permission).

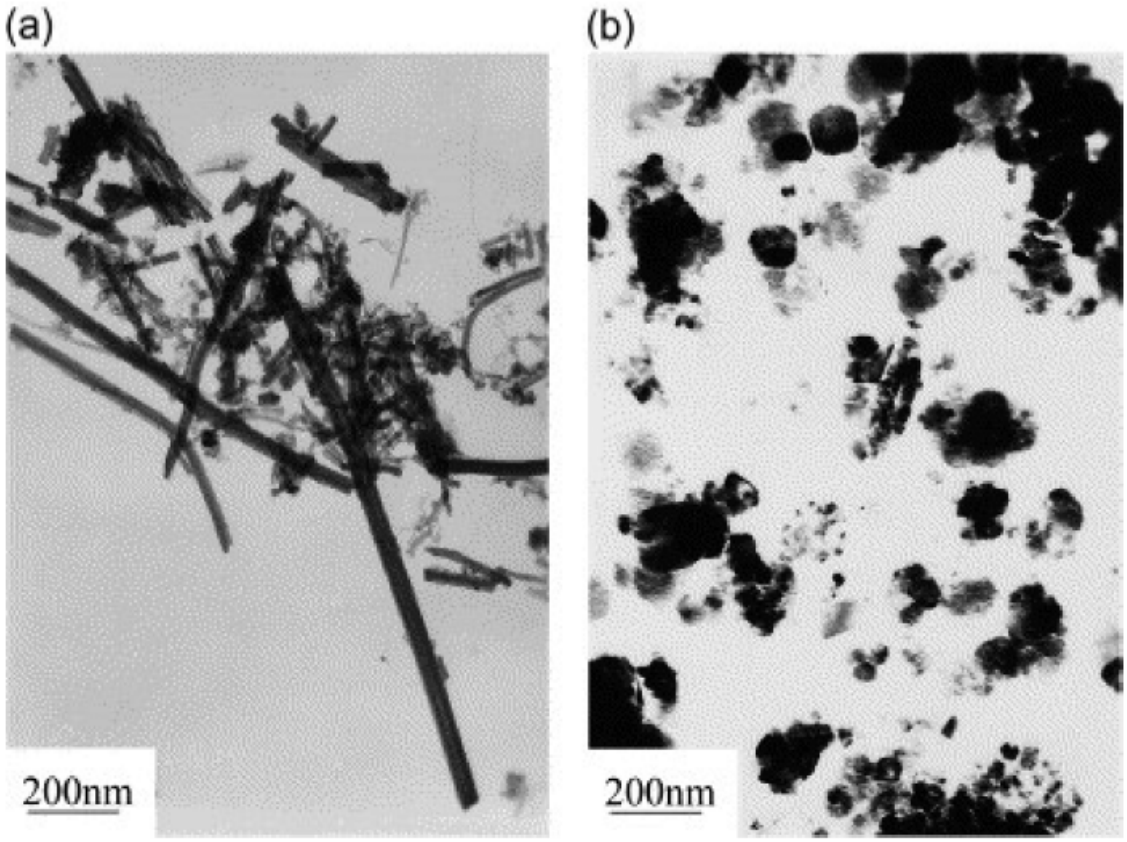

Figure 8. Scanning electron microscopy (SEM) images of FeS_2 SINPs prepared from a mixture of $FeSO_4$ with $Na_2S_2O_3$ and elemental S in water for 24 h at 200°C for 24 h (reproduced from Wu et al.[147] with permission).

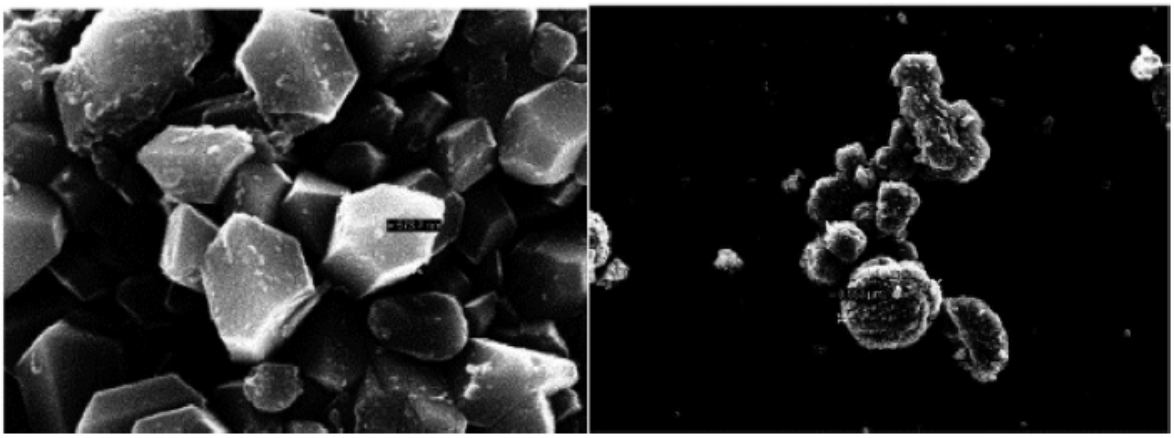

Figure 9. TEM images showing the biosynthesis of FeS nanoparticles by *S. oneidensis* (A) SINPs on the cell surface and (B) SINPs suspended in the medium (electron diffraction pattern shown inset) (reproduced from Xiao et al.[127] with permission).

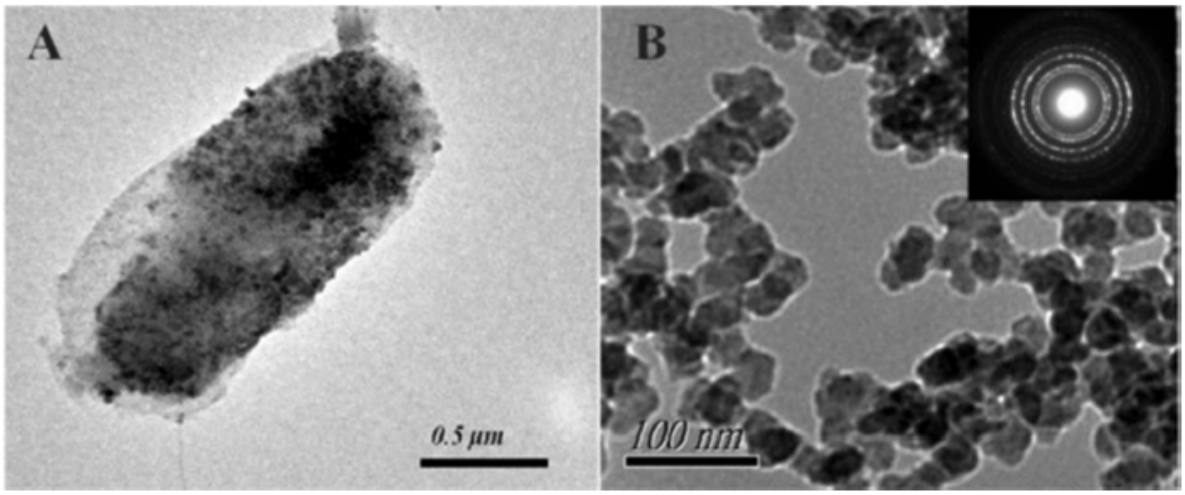

Figure 10. Schematic of a possible formation mechanism of FeS_2 nanowires and nanotubes by sol−gel and sulfurization (adapted from Li et al.[49] with permission).

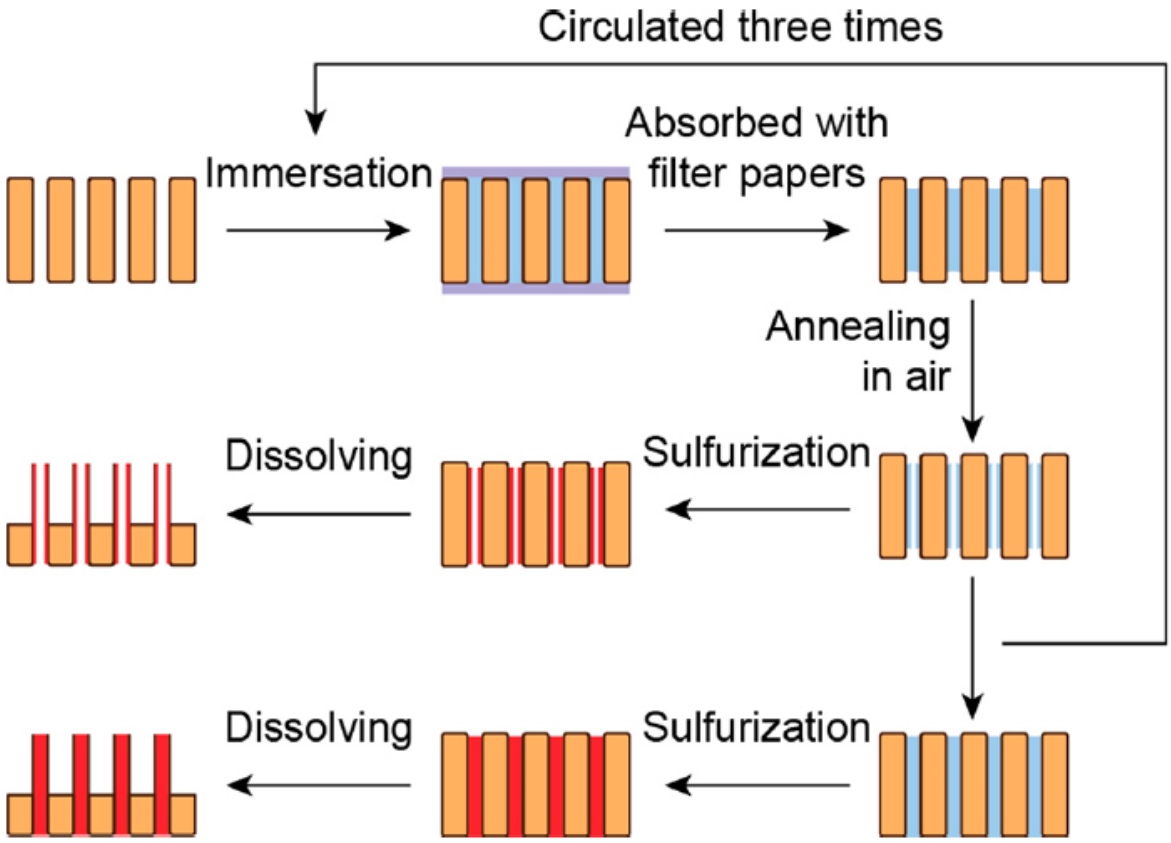

Table 1. Summary of Types and Characteristics of Sulfur-Bearing Iron Nanoparticles (SINPs)

SINP Type	Characteristics
FeS, mackinawite and troilite (approximate FeS)	Iron(II)sulfide (FeS) is not normally stable in an amorphous form. Cubic FeS_c has a cubic *F43m* structure and is not found in nature because it easily converts to mackinawite.[19,20] Mackinawite, expressed in the formula FeS_m, comprises Fe atoms surrounded by four sulfur atoms in a nearly perfect tetrahedron structure,[21] forming a tetragonal *P4/nmm* structure.[19] It is a widespread metastable mineral in low-temperature environments. FeS can also be found in nature as troilite (FeS_t), a near stoichiometric iron sulfide with a hexagonal $P\bar{6}2c$ structure.[19] It is the stoichiometric end member of the pyrrhotite mineral group having antiferromagnetic properties at ambient temperature.[22]
Pyrrhotite ($Fe_{1-x}S$)	Pyrrhotite ($Fe_{1-x}S$, where x = 0 to 0.13) minerals are non-stoichimetric variants of FeS which exist as monoclinic (e.g., *A2/a*) or hexagonal (e.g., *P6/mmc*) structures[19] or trigonal phases.[23] It is the ordered omission of Fe that produces superstructures that range from hexagonal to monoclinic.[24] The monoclinic structure (often denoted as Fe_7S_8, but with a wide compositional range) contains alternating layers of full iron sites and layers of sites with iron vacancies. Pyrrhotite with a hexagonal structure (i.e., the nickel arsenide (NiAs) structure) will distort into a monoclinic structure if the vacancy content is greater than 0.11 per formula unit.[25] Hexagonal primary pyrrhotite can be partially oxidized when exposed to oxygen, forming iron-deficient secondary pyrrhotite.[23]
Greigite (Fe_3S_4)	Greigite (Fe_3S_4) has a cubic *Fd3m* structure[19] and is the iron sulfide counterpart of spinel magnetite (Fe_3O_4); although greigite is a normal metal, magnetite is only half-metallic.[26] The unit cell of the stoichiometric inverse spinel greigite structure contains 32 sulfur atoms and 24 iron atoms,[27,28] with two sublattices of iron atoms with Fe^{3+} ions occupying tetrahedral A-sites and Fe^{2+} and Fe^{3+} ions occupying octahedral B-sites.[29] While greigite is thermally stable at ambient temperature, it will break down to form pyrrhotite when heated and slowly dissolves in hydrofluoric acid or warm hydrochloric acid.[27] The relative instability of greigite has resulted in it being less well studied than magnetite, but engineered greigite is now receiving greater interest owing to its complex magnetic properties.[30]
Pyrite (FeS_2)	Pyrite has the composition of FeS_{2p} and forms in a cubic *Pa3* structure.[19] It is one of the most abundant minerals of the Earth's surface.

Table 2. Selected Sulfur-Bearing Fe-Rich Nanoparticle Synthesis Procedures and Approaches

SINP Type	Synthesis method	Reference
biochar-supported FeS	$FeSO_4 \cdot 7H_2O$ was mixed with carboxymethyl cellulose (CMC) and biochar. Na_2S solution was added dropwise to the solution.	121
$Cd_xZn_{1-x}S@Fe_3S_4$	Iron triacetylacetonate was dissolved in ethylene glycol solution. Thioacetamide was added and allowed to react for 2 h before $Cd(NO_3)_2$ and $Zn(NO_3)_2$ were added.	122
CMC-stabilized FeS	CMC solution was mixed with $FeSO_4$ and Na_2S solutions.	123
Fe/FeS	Fe and S powders were milled together and heat treated at 1123 K.	124
Fe_3S_4-C	$FeCl_3$ and thioacetamide were dissolved in ethylene glycol and glucose added.	125
FeS	$FeSO_4$ aqueous solution was mixed with Na_2S solution. Carboxymethyl cellulose (CMC) was added as a stabilizer.	126
FeS	Lactate was added as an electron donor, with thiosulfate added as an electron acceptor and sulfur source. Naphthol green B was also added.	127
FeS-coated ZVI	$FeSO_4$ was mixed with $NaBH_4$ and thioacetamide.	128
FeS-stabilized with biopolymers	Biopolymers were extracted from *basidiomycetous* fungus (*Itajahia* sp.).	129
FeS/FeSe	Trinuclear iron(III) precursor complex reacted with thiourea.	130
FeS_2	$FeCl_2 \cdot 4H_2O$ was mixed with $Na_2S_2O_3$ and heated at 200°C for 24 h.	61
FeS_2	High-energy mechanical ball milling occurred.	131
FeS_2	Plasma-treated pyrite was prepared with an Ar glow discharge plasma.	132
FeS_2	Pyrite ore was treated with glow discharge plasma in a N_2 atmosphere.	133
FeS_2	Reaction of $FeSO_4 \cdot 7H_2O$ with $Na_2S_2O_3 \cdot 5H_2O$ occurred.	134
FeS_2	$FeCl_2$ and oleylamine were mixed, followed by sulfur injection and heating to 220°C.	135
magnetic FeS	Biosynthesis with *Desulfovibrio vulgaris* Miyazaki occurred.	136
magnetic sulfide-modified ZVI	Sodium borohydride and dithionite were added to $FeCl_3$ solution by titration.	137
pyrrhotite	Natural pyrite was calcined at a temperature of 600 °C for 1 h.	138
pyrrhotite (Fe_7S_8)	Reaction between iron chloride ($FeCl_3$) and thiourea occurred.	139
sulfide-modified Fe	Dithionite was added to a sodium borohydride solution. Nano-SiO_2 was added to the solution. After that, the mixture was titrated into a $FeCl_3$ solution.	140
sulfide-modified ZVI	Sodium borohydride and dithionite were added to an $FeCl_3$ solution in a dropwise manner.	141
sulfur-modified Fe	Iron and sulfur were mixed in an exothermic reaction.	142